

The Collisional Evolution of the Main Asteroid Belt

William F. Bottke

Southwest Research Institute/Institute for the Science of Exploration Targets (ISET)

Miroslav Brož

Charles University

David P. O'Brien

Planetary Science Institute

Adriano Campo Bagatin

Universidad de Alicante

Alessandro Morbidelli

Lagrange Laboratory, Université Côte d'Azur, Observatoire de la Côte d'Azur, CNRS

Simone Marchi

Southwest Research Institute/Institute for the Science of Exploration Targets (ISET)

Collisional and dynamical models of the main asteroid belt allow us to glean insights into planetesimal- and planet-formation scenarios as well as how the main belt reached its current state. Here we discuss many of the processes affecting asteroidal evolution and the constraints that can be used to test collisional model results. We argue the main belt's wavy size-frequency distribution for diameter $D < 100$ -km asteroids is increasingly a byproduct of comminution as one goes to smaller sizes, with its shape a fossil-like remnant of a violent early epoch. Most $D > 100$ -km asteroids, however, are primordial, with their physical properties set by planetesimal formation and accretion processes. The main-belt size distribution as a whole has evolved into a collisional steady state, and it has possibly been in that state for billions of years. Asteroid families provide a critical historical record of main-belt collisions. The heavily depleted and largely dispersed "ghost families," however, may hold the key to understanding what happened in the primordial days of the main belt. New asteroidal fragments are steadily created by both collisions and mass shedding events via YORP spinup processes. A fraction of this population, in the form of $D < 30$ km fragments, go on to escape the main belt via the Yarkovsky/YORP effects and gravitational resonances, thereby creating a quasi-steady-state population of planet-crossing and near-Earth asteroids. These populations go on to bombard all inner solar system worlds. By carefully interpreting the cratering records they produce, it is possible to constrain how portions of the main-belt population have evolved with time.

1. INTRODUCTION

The main asteroid belt is a living relic. It contains a record of what happened to the solar system in terms of bombardment since the planet-formation epoch. Ongoing collisional and dynamical evolution processes, however, are slowly obscuring the traces left behind. The goal of modeling efforts is to use all possible observational data to discern the initial conditions and evolution processes that occurred during and after the planet-formation epoch. For example, the questions one can probe with main-belt constraints include the nature

and mass of planetesimals inside Jupiter's orbit, the timing of Jupiter's formation, the distribution of volatiles in the inner solar system, the size distribution produced during planetary accretion, the presence of planetary embryos inside Jupiter's orbit, the migration of the giant planets and whether sweeping resonance ever crossed the main belt, the degree of material mixing that occurred between the feeding zones, etc.

The problem is that our uncertainties about planet-formation processes and giant planet migration feed back into the assumptions made for our collisional-evolution models of the asteroid belt. If we do not know what happened when, it

is often difficult to impossible to find unique solutions. On the other hand, the main belt provides powerful constraints, and sometimes even order-of-magnitude solutions are useful at testing planet-formation scenarios. As a result, many main-belt-evolution scenarios have been investigated over the last several decades. The latest thinking on the primordial dynamical evolution of the main belt is discussed in the chapter by Morbidelli et al. in this volume.

A key issue for many evolution models concerns the so-called mass deficit of the main belt (e.g., *Morbidelli et al., 2009*). Consider that the total mass of the main asteroid belt, which is dominated by the masses of the largest asteroids, is $\sim 5 \times 10^{-4} M_{\oplus}$ (*Krasinsky et al., 2002; Somenzi et al., 2010; Kuchynka and Folkner, 2013*). This value is tiny compared to the mass of solids thought to exist in the same region at the time of planetesimal formation. For example, the minimum mass solar nebula (*Weidenschilling, 1977*) suggests that 1–2.5 M_{\oplus} of solid material once existed between 2 and 3 AU. If most of the solids ended up in planetesimals, the main-belt region could potentially be deficient in mass by a factor of >1000 . These values have been used to argue that the asteroid belt has lost more than 99.9% of its primordial mass (e.g., *Morbidelli et al., 2009*). The critical unknown here is the efficiency and nature of planetesimal formation itself, which is discussed in the chapter by Johansen et al. in this volume.

If so much mass once existed in the primordial main-belt region, collisional evolution, dynamical removal processes, or some combination of the two were needed to get rid of it and ultimately produce the current main-belt population. For some time, many attempts were made to account for the mass deficit by collisions alone; see *Davis et al. (2002)* for a review of work up to the time of *Asteroids III*. Essentially, there are two key problems with this scenario. First, it is difficult for collisions alone to grind away the main-belt size distribution predicted by accretion models without blasting away Vesta's basaltic crust or producing size-frequency distributions (SFDs) that are inconsistent with the observed main-belt SFD (e.g., *Davis et al., 1985*). Second, collisional models employing disruption scaling laws based on numerical hydrocode simulations of asteroid collisions (e.g., *Benz and Asphaug 1999*) cannot break up enough $D > 100$ -km asteroids to reproduce the observed population; too many large objects are left behind (e.g., *Bottke et al., 2005a,b*). Taken together, these outcomes suggest that either dynamical removal of asteroids has played a powerful role in allowing the population to reach its current state (see the chapter by Morbidelli et al. in this volume), or that the main-belt SFD for the largest asteroids has not changed very much since planetesimal formation.

For the former, several dynamical scenarios have been suggested to remove most of the primordial main belt's mass (see the chapter by Morbidelli et al. in this volume). For example, planetary embryos may have initially formed in the main-belt region (e.g., *Petit et al., 2002*, for a review; see also *Chambers and Wetherill, 1998, 2001; O'Brien et al., 2006, 2007*). As they gravitationally excited themselves and the surrounding planetesimals, most of these bodies escaped,

thereby naturally creating much of the main-belt mass deficit. In a second example, Jupiter gravitationally interacts with the gas disk and migrates across the main-belt region (*Walsh et al., 2011*). This so-called Grand Tack scenario allows Jupiter to do the job of scattering embryos and planetesimals out of the main-belt region. The key similarity of both examples is that planetesimals dynamically excited out of the main belt have the opportunity to slam into the survivors left behind (along with leftover planetesimals already on planet-crossing orbits) (*Bottke et al., 2005b; O'Brien and Greenberg, 2005; O'Brien et al., 2006; Davidson et al., 2013*). This allows these dynamical models to be at least partially tested against main-belt asteroid and meteoritical constraints.

An alternative scenario is to assume that planetesimal and planet formation works differently than has been assumed in existing scenarios, and that the quantity of planetesimals in the main-belt region was never more than a few times the present-day population (e.g., *Levison et al., 2015a,b*). This would remove the need for a mass deficit. This new scenario invokes a process called “pebble accretion” that describes how planetesimal growth rates are governed by the way in which small particles are affected by gas drag in the solar nebula near a growing body (see the chapter by Johansen et al. in this volume). In brief, planetesimals embedded in a population of “pebbles,” whose sizes are debated, can grow very quickly because of a newly discovered mode of accretion aided by aerodynamic drag on the pebbles themselves. If a pebble's aerodynamic drag stopping time is less than or comparable to the time for it to encounter a growing body, such as a planetary embryo, then it is decelerated with respect to the planetary embryo and becomes gravitationally bound. After capture, the pebble spirals inward and is accreted. If pebble-accretion scenarios are found to be valid, early collisional evolution in a low-mass main belt might be dominated by leftover planetesimals that strike from planet-crossing orbits.

Beyond the earliest times, one must also consider whether the main-belt population was affected by giant planet migration taking place after the solar nebula had completely dissipated. In a popular suite of scenarios referred to as the Nice model (see the chapter by Morbidelli et al. in this volume), the giant planets undergo a gravitational instability long after the formation of the first solids. Ice giants like Uranus and Neptune migrate across a massive primordial disk of comets, scattering most across the solar system. Some of these bodies will slam into main-belt asteroids (*Brož et al., 2013*). As the gas giants migrate to their current orbits, secular resonances produced by the giant planets also jump to new positions, and some will interact with the primordial main-belt population. This may cause the primordial main belt to lose some of its mass (*Gomes et al., 2005; Brasser et al., 2009; Morbidelli et al., 2010; Minton and Malhotra, 2009, 2011*). At the same time, it may also trap some destabilized comets within this region on stable orbits (*Levison et al., 2009*). The new home for certain secular resonances may even destabilize a putative stable extension of the main belt that once existed between 1.7 and 2.2 AU (*Bottke et al.,*

2012). It is likely that evidence for or against these possibilities can still be found in the asteroidal impact record, provided we know what to look for there.

The question is how to test these concepts with what we know about asteroids and the main belt itself, and whether the constraints we know about today are sufficient to eliminate various planet-formation and evolution scenarios. To answer this, we first must examine the processes affecting asteroidal collisional evolution, and what would need to be incorporated into a comprehensive collisional-evolution model (section 2). Next, we need to discuss the constraints that can be reasonably brought to bear on this problem (section 3). Only then can we discuss what we have learned from existing models (section 4). We also refer the interested reader to the excellent reviews of historical collisional evolution work provided in previous *Asteroids* volumes by *Davis et al.* (1979, 1989, 2002), and to a much more limited literature review in *Bottke et al.* (2005a). As much as possible, we have tried to avoid duplication with these works while keeping this chapter self-contained.

2. PROCESSES AFFECTING MAIN-BELT EVOLUTION

At the most basic level, main-belt collisional-evolution models involve the solution of a straightforward differential equation, although the details can become complicated and somewhat messy from an accounting standpoint. The input is an initial SFD for the asteroid belt denoted as $N(D, t)$, with the bodies binned in logarithmic intervals as a function of diameter. The goal of the solution is to compute the time rate of change in the population per unit volume of space over a size range between diameter D and $D + dD$. In a schematic form, it can be written as

$$\frac{\partial N}{\partial t}(D, t) = -I_{\text{COLL}} + I_{\text{FRAG}} - I_{\text{DYN}} \quad (1)$$

Here I_{COLL} is the net number of bodies that leave between D and $D + dD$ per unit time from collisions (i.e., it is a “sink” for bodies in the SFD). The net number of collisions taking place at every time step is calculated by determining how many projectiles from other size bins are capable of producing either a cratering or a catastrophic disruption event among bodies between D and $D + dD$. Note that other mass loss processes can be included here as well, such as the loss of material via nongravitational YORP torques, which can spin up asteroids fast enough that they shed mass (see the chapter by Vokrouhlický et al. in this volume and section 2.5 below).

The results of the I_{COLL} calculation are sent to the function I_{FRAG} , which describes the number of bodies entering a given size bin per unit time that were produced by the fragmentation of larger bodies (i.e., it is a “source” for bodies in the SFD). This allows large asteroids to act as a reservoir for smaller bodies, with collisional evolution or some other process liberating fragments over time.

Finally, the equation accounts for I_{DYN} , which is the number of bodies lost from a given size bin via dynamical processes, such as an object escaping through a dynamical resonance (i.e., it is a “sink” for bodies in the SFD). Note that I_{DYN} is often enacted over the entire main-belt SFD, which is reasonable for global dynamical mechanisms like sweeping resonances or migrating planets but is less accurate for bodies escaping from specific main-belt regions via dynamical resonances (e.g., the v_6 secular resonance along the inner edge of the main belt; the 3:1 mean-motion resonance with Jupiter at 2.5 AU).

In the sections below, we discuss the many parameters and mechanisms needed to understand and create these functions within a collision evolution model.

2.1. Asteroid Collision Probabilities

A necessary component to determining the collisional evolution of a population is to compute the impact probabilities and relative velocities between all possible pairs of bodies. These values are used to estimate the interval between targets and projectiles of different sizes striking one another as well as the effects of those collisions. The most common value used in these cases is the intrinsic collision probability P_i , defined as the likelihood that a single projectile will hit the target over a unit of time and cross-sectional area, and the mean impact velocity V_{imp} between the pair (e.g., *Öpik*, 1951; *Wetherill*, 1967; *Farinella and Davis*, 1992; *Bottke et al.*, 1994).

To get these values for the present-day main belt, *Bottke et al.* (1994) took a representative sample of main-belt asteroids [e.g., 682 asteroids with $D > 50$ km as defined by *Farinella and Davis* (1992)] and calculated P_i and V_{imp} between all possible pairs of asteroids, assuming fixed values of semimajor axis, eccentricity, and inclination (a, e, i). A common approximation made here is that the orbits can be integrated over uniform distributions of longitudes of apsides and nodes because secular precession randomizes their orbit orientations over $\sim 10^4$ -yr timescales. After all possible orbital intersection positions for each projectile-target pair were evaluated and weighted, they found that main-belt objects striking one another have $P_i \sim 2.9 \times 10^{-18} \text{ km}^{-2} \text{ yr}^{-1}$ and $V_{\text{imp}} \sim 5.3 \text{ km s}^{-1}$. These values are fairly reasonable given what we know about the main-belt population today, and comparable values can be found in many works (e.g., *Farinella and Davis*, 1992; *Vedder*, 1998; *dell’Oro and Paolicchi*, 1998; *Manley et al.*, 1998). Estimates for different portions of the main-belt population striking one another have been reported as well (e.g., *Levison et al.*, 2009; *Cibulkova et al.*, 2014).

To model collisional evolution in the primordial asteroid belt requires that certain assumptions be made about the excitation of asteroid belt bodies at that time. For example, the process that caused the main-belt population to become dynamically excited (see the chapter by Morbidelli et al. in this volume) should have also driven many primordial main-belt asteroids onto planet-crossing orbits. While their orbits

were short lived, their higher eccentricity and inclinations would have allowed them to strafe the surviving main belt asteroids at $V_{\text{imp}} > 10 \text{ km s}^{-1}$ for tens of millions of years (e.g., *Bottke et al.*, 2005b; *Davidson et al.*, 2013; *Marchi et al.*, 2013). Moreover, if the primordial main belt once had considerably more mass, as discussed in section 1, these departed bodies could be responsible for a considerable amount of collisional evolution in the main belt.

A related issue is that the primordial main belt has likely been struck by sizable but transient populations on planet-crossing orbits, such as leftover planetesimals (*Bottke et al.*, 2006, 2007), ejecta from giant impacts in the terrestrial planet region (*Bottke et al.*, 2015b), comet-like planetesimals dispersed from the primordial disk during giant planet migration (*Brož et al.*, 2013), and Jupiter–Saturn-zone planetesimals pushed into the inner solar system via giant planet migration and/or evolution (*Walsh et al.*, 2011; *Turrini et al.*, 2011, 2012). Most of these dramatic events are thought to take place during the first 500 m.y. of solar system history. The nature and evolution of these populations is uncertain, such that dynamical models are needed to set limits on what they were plausibly like (see the chapter by Morbidelli et al. in this volume). Under certain conditions, they could also account for abundant collisional grinding in the main belt.

In all cases, dynamical models are needed to allow the computation of P_i and V_{imp} between the impacting bodies and the main-belt targets. From there, it is a matter of estimating the initial sizes of the populations, how fast they disperse, and how the populations undergo collisional evolution among themselves.

2.2. Asteroid Disruption Scaling Laws

A second key issue to modeling asteroid collisional evolution concerns the disruption scaling law. This is commonly referred to as the critical impact specific energy Q_D^* , the energy per unit target mass delivered by the projectile required for catastrophic disruption of the target (i.e., such that one-half the mass of the target body escapes). A considerable amount has been written about the value of Q_D^* (e.g., reviews in *Holsapple et al.*, 2002; *Asphaug et al.*, 2002; *Davis et al.*, 2002; see also *Leinhardt and Stewart*, 2009; 2012), and the latest on the computation of this value can be found in the chapters in this volume by *Jutzi et al.* and *Michel et al.* For these reasons, we only briefly review the main issues here.

Using Q_D^* , the diameter of a projectile d_{disrupt} capable of disrupting a target asteroid (D_{target}) can be estimated as

$$d_{\text{disrupt}} = \left(2Q_D^*/V_{\text{imp}}^2\right)^{1/3} D_{\text{target}} \quad (2)$$

where V_{imp} is the impact velocity. We assume here that the target and projectile have the same bulk density, although that is by no means assured. Small asteroids are considered part of the “strength-scaling” regime, where the fragmentation of the target body is governed by its tensile strength,

while large asteroids are considered part of the “gravity scaling” regime, where fragmentation is controlled by the self-gravity of the target (see section 4.1). Laboratory experiments and hydrocode modeling work discussed in the references above suggest the transition between the regimes occurs in the range $100 < D < 200 \text{ m}$ (Fig. 1).

Testing what impacts do to undamaged targets with basalt-like physical properties, *Benz and Asphaug* (1999) found that the mass of the largest remnant M_{LR} after a collision can be fitted as a function of Q/Q_D^* , where the kinetic energy of the projectile per unit mass of the target is denoted by Q

$$M_{\text{LR}} = \left[-\frac{1}{2}\left(\frac{Q}{Q_D^*} - 1\right) + \frac{1}{2}\right] M_T \quad (3)$$

for $Q < Q_D^*$, and

$$M_{\text{LR}} = \left[-0.35\left(\frac{Q}{Q_D^*} - 1\right) + \frac{1}{2}\right] M_T \quad (4)$$

for $Q > Q_D^*$, where M_T is the target mass. Whenever M_{LR} in equation (3) turns out to be negative, one can assume that the target has been pulverized, such that all its mass is lost below some minimal mass threshold.

A missing aspect of this discussion is that asteroids have a wide range of physical properties and therefore may disrupt very differently than the idealized bodies used in numerical hydrocode runs. We refer the reader to the chapters in this

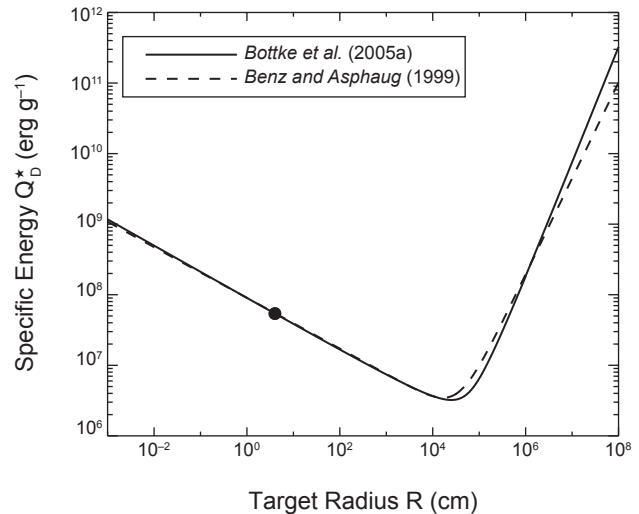


Fig. 1. The critical impact specific energy Q_D^* defined by *Benz and Asphaug* (1999). This function is the energy per unit target mass delivered by the projectile that is required for catastrophic disruption of the target, such that one-half the mass of the target body escapes. The dashed line is the function derived by *Bottke et al.* (2005a) for their modeling results. Both functions pass through the normalization point (Q_D^* , D) set to $(1.5 \times 10^7 \text{ erg g}^{-1}, 8 \text{ cm})$, which was determined using laboratory impact experiments (e.g., *Durda et al.*, 1998).

volume by Jutzi et al. and Michel et al., who discuss recent advances made in this area. Here we point out that all collisional models must, by necessity, make approximations to deal with complicated systems. This has led many modelers to assume that all asteroids (e.g., monoliths, rubble piles, etc.) follow the exact same Q_D^* functions for disruption. While this approach may be more accurate than one might expect (see results in the chapters in this volume by Jutzi et al. and Michel et al.), future collision evolution models will need to consider how specific asteroid types react to impacts. In addition, the influence of asteroid spin on Q_D^* has not been investigated so far in the hypervelocity impact regime, and it is likely that a spinning asteroid responds differently to an impact than a nonspinning one, as found in low-speed impacts between self-gravitating aggregates (e.g., Ballouz et al., 2014).

In practice, this will mean sorting all asteroids into broad categories that can be treated by individual Q_D^* functions. One possible way to divide them up would be by spectral signatures, such as the S-, C-, and X-complexes (see the chapter by DeMeo et al. in this volume). Within the complexes, bodies might share similar albedos (see chapters by Mainzer et al. and Masiero et al.), bulk densities and porosities (see chapter by Scheeres et al.), compositions, and so on. Differences between categories could then be dealt with in a logical fashion. For example, we know that C-complex bodies often have lower bulk densities and higher porosities than S-complex bodies, and studies of primitive carbonaceous chondrites suggest many are structurally weaker and have different grain structures as well (e.g., Britt et al., 2002). Whether this affects their Q_D^* function will then need to be determined by laboratory impact experiments and numerical hydrocode simulations of asteroid collisions. There will also be the issue of how to treat the exceptional cases (e.g., the X-complex include a wide range of asteroid types, internal structures, compositions, and bulk densities).

The hope is that this kind of work will eventually lead us to an understanding of the SFDs of different asteroid complexes and how they have changed over time. By getting the details right, it may be possible to ask more interesting questions about how the main belt reached its current state. Even the assumption that all asteroids should be placed into the S- or C-complexes, where their physical properties would be treated differently, would be an advance over current model assumptions.

2.3. Asteroid Fragmentation

One of the most difficult issues to deal with in any collisional evolution model is the treatment of the fragment SFD created when two bodies slam into one another. Given the wide range of parameters that could be involved in any collision, such as impact velocity, projectile and target sizes, impact angle, projectile and target properties, etc., it is a somewhat quixotic task to try to generate a “one size fits all” recipe capable of reproducing the outcomes of all meaningful cratering and catastrophic disruption events that could have ever taken place in the asteroid belt.

Comprehensive experimental work has been carried out over the last several decades on this subject. Studies based on hypervelocity laboratory impacts have provided threshold specific energies for shattering (Q_S^*) among a wide range of materials, and scaling theories including strain-rate and gravity-scaling effects allow one to extrapolate those results to multi-kilometer-sized asteroids (Holsapple et al., 2002; chapter by Michel et al. in this volume). They show that Q_S^* and Q_D^* coincide in the strength regime, but $Q_S^* < Q_D^*$ in the gravity regime and the minimum energy to disperse a given target can be expressed as the sum of the energy needed to shatter the body and the energy required to disperse the fragments. In this way, once the comparison between the impact specific energy and the value of Q_S^* is made, it is possible to determine whether the impact will be a cratering or a disruption event. In both cases the size distribution of the new fragments can potentially be calculated (e.g., Petit and Farinella, 1993). The critical quantity that discriminates cratering from shattering is the mass fraction between the largest fragment (M_{LR}) and the target (M_T), which is given by

$$f_{LF} = \frac{M_{LF}}{M_T} = 0.5 \left(\frac{Q_S^*}{E/2} \right)^{1.24} \quad (5)$$

In the case of a barely shattering impact event, $f_{LF} = 0.5$. Using Q_S^* instead of Q_D^* has the advantage of allowing one to calculate how many fragments are reaccumulated by the self-gravity of the non-escaping fragments (Campo Bagatin et al., 1994b).

One must also consider that many $D < 100$ -km asteroids are likely to be second-generation gravitational aggregates. Campo Bagatin et al. (2001) tracked this aspect of collisional evolution, and found that the amount of reaccumulated mass for each object was enough that it could affect both the target body’s Q_D^* function as well as the fragment SFD created in an impact. Note that the lower size limit on gravitational aggregates is unknown; some meter-sized bodies may possibly be held together by cohesive forces (see the chapter by Scheeres et al. in this volume). Ultimately, little is known about the mass distribution of the fragments — aggregates themselves or single coherent components — coming out of a disrupting impact on a gravitational aggregate, although insights into this can potentially be gleaned from numerical hydrocode experiments of collisions on rubble-pile asteroids (Benavidez et al., 2012; see the chapter by Michel et al. in this volume).

Gravitational aggregates may also be produced by multiple subcatastrophic collisions, which may lead to the same result as a single shattering collision, provided their total energy is equivalent to the energy of the shattering event (Housen, 2009). This could mean some second-generation asteroids are gravitational aggregates with limited macroporosity, due to the fact that fragments did not get enough kinetic energy to be jumbled and reshuffled. How these results feed into the creation of new fragment SFDs are uncertain. Improvements in this area, along the lines of an

updated *Campo Bagatin et al.* (2001) model, could help to better characterize collisional evolution in the main belt.

These issues influence the internal structure of asteroids. This may explain why mass and volume measurements of asteroids indicate a wide range of internal macroporosities for S- and C-complex asteroids (see the chapter by Scheeres et al. in this volume). Unfortunately, porosity is only a partial indicator of internal structure, as it is largely independent of the sizes of components. Porosity also hides the absolute sizes of components and their distribution. A porous gravitational aggregate might have a substantial microporosity (e.g., individual constituents with a fairy-castle structure) and/or a sizable macroporosity (e.g., large fragments and empty space near the contact points covered by regolith). The fact that many main-belt asteroids may have unusual internal structures makes it imperative that we obtain more ground truth on how real asteroids are affected by collisions.

Beyond this, it is important to recognize that our asteroid belt has been subject to an enormous number of stochastic events, and information about the fragments produced by ancient collisions has been lost by subsequent collisional and dynamical processes. This means the initial conditions for ancient family-forming events or even large cratering events (see the chapters by Asphaug et al. and Nesvorný et al. in this volume) may never be precisely known (see the chapters by Jutzi et al. and Michel et al.). A good example of this is the impact event that created the 400-km Veneneia basin on (4) Vesta; the basin has been partially buried/destroyed by the nearby Rheasilvia basin-formation event (*Schenk et al.*, 2012; see the chapter by Russell et al.).

Given these limitations, realistic modelers do the best they can with what they have. This means choosing parameters and formalism that are reasonable within the bounds of what is known and testing their results against the available constraints. The interpretation of even good matches, though, must always be met with some skepticism and wariness. Moreover, a careful modeler must also run simulations over numerous trials in an attempt to characterize how outcomes may have been affected by chance events (e.g., the disruption of a large asteroid at a strategic time or place may allow a model run to match constraints, yet this kind of event may not have happened in our asteroid belt).

To this end, modern collisional-evolution models have folded into their codes outcomes of numerical smoothed particle hydrocode (SPH) simulations that account for at least some of the parameters described above. For example, *Morbidelli et al.* (2009) constructed an algorithm that reproduced the fragment size distribution of the SPH results determined by *Durda et al.* (2004, 2007), who conducted a large number of collision simulations of projectiles of various masses and velocities striking 100-km-diameter asteroids. They found that most catastrophic collisions produce fragment SFDs that have a continuous, steep power-law size distribution starting from a single large fragment that is well separated in size from that of the largest remnant of the target.

The mass of the largest fragment and the slope of the power-law SFD in each of the experiments from *Durda et al.*

(2007) was described as a function of the ratio Q/Q_D^* that characterized each experiment

$$M_{LF} = 8 \times 10^{-3} \left[\frac{Q}{Q_D^*} \exp \left(- \left(\frac{Q}{4Q_D^*} \right)^2 \right) \right] (M(i) + M(j)) \quad (6)$$

for the mass of the largest fragment and

$$q = -10 + 7 \left(\frac{Q}{Q_D^*} \right)^{0.4} \exp \left(- \frac{Q}{7Q_D^*} \right) \quad (7)$$

for the slope of the cumulative power-law size distribution of the fragments. These equations represent empirical fits to the numerical hydrocode data. Note that comparable functions were created by *Cibulková et al.* (2014) from the rubble-pile impact simulation results of *Benavidez et al.* (2012). These equations were incorporated into their collisional-evolution models.

For fragment SFDs with very steep slopes, equations (5) and (6) can easily exceed the mass of the projectile and target, which is nonphysical. To avoid this problem, it is assumed that the fragment SFDs bend to shallower slopes at small sizes, although the precise diameter where this takes place is unknown; it is beyond the resolution limit of existing numerical hydrocode impact simulations.

It can be shown that the derived fragment SFDs from these simulations reproduce many attributes of observed asteroid families (*Durda et al.*, 2007). With that said, however, collisional outcomes and fragment SFDs are strongly affected by the target's gravitational forces; this means the impact outcomes onto 400-km targets differ from those of 100-km targets in terms of Q/Q_D^* (P. Benavidez, personal communication). The same is probably true for smaller targets as well. Major advances in this area will therefore come from those modelers who employ fragment SFDs appropriate for their target sizes.

A final interesting issue here is that analytical and numerical results suggest the final equilibrium main-belt SFD is often found to be relatively insensitive to the details of the fragmentation law (e.g., *Davis et al.*, 2002; *O'Brien and Greenberg*, 2003, 2005; *Bottke et al.*, 2005a,b; *Morbidelli et al.*, 2009). This statement is mainly based on experience, and it needs to be better quantified by modeling work. We suggest that while the fragmentation laws used are important, many are unlikely to dramatically change the equilibrium results. On the other hand, the choice of fragment SFD for given breakups will be important for investigating asteroid families and transient perturbations to the main-belt SFD.

2.4. Dynamical Depletion of Main-Belt Asteroids by the Yarkovsky Effect

As described in the chapter in this volume by *Vokrouhlický et al.*, $D < 30$ -km asteroids in the main belt slowly drift inward toward or outward away from the Sun in semimajor

axis by Yarkovsky thermal forces. This allows some of them to reach resonances with the planets that drive them onto planet-crossing orbits, thereby allowing them to escape the main-belt region altogether. Additional mobility is provided by encounters with big asteroids like (1) Ceres and (4) Vesta, although the net effect of this mechanism is fairly modest (e.g., Carruba et al., 2003, 2013).

The Yarkovsky effect, working in concert with resonances, can therefore be considered a “sink” for small main-belt asteroids. Their depletion should feed back into the collisional evolution of the main belt itself (i.e., fewer smaller bodies means fewer cratering and disruption events among larger bodies). It also means that the near-Earth asteroid (NEA) population could be considered a short-lived component of the main-belt population. This allows the NEA SFD to constrain collisional and dynamical evolution within the main belt, provided the modeler understands the translation between the main belt and NEA SFDs (e.g., Morbidelli and Vokrouhlický, 2003).

The challenging part of this is to quantify the nature of small-body populations lost over time via the Yarkovsky effect and resonances. Consider the following:

- Every major main-belt resonance has a different character in its ability to produce long-lived near-Earth objects (NEOs) (e.g., Gladman et al., 1997; Bottke et al., 2006).
- The flux of asteroids reaching dynamical resonances may change over time as a consequence of asteroid family-forming events. Large asteroid families can produce enormous numbers of fragments, while smaller ones that disrupt in strategic locations next to key “escape hatches” may also influence the planet-crossing population for some interval (Nesvorný et al., 2002).
- The dynamical evolution of $D < 1$ -km asteroids is poorly constrained because these bodies are below the observational detection limit of most surveys (e.g., Jedicke et al., 2002; see also the chapter by Jedicke et al. in this volume). Moreover, these bodies are also the most susceptible to YORP thermal torques, which can strongly affect their drift direction and evolution (see next section).

So far, no one has yet attempted to model all these factors and include them into an algorithm suitable for insertion into a collisional evolution code. It is a necessary but daunting task to do this correctly, given the current state of our knowledge of how the Yarkovsky/YORP effects modify the orbits, sizes, and shapes of small asteroids.

Instead, the best that has been done to date has been to generate loss rates for the asteroid belt that produce a steady-state population of NEOs (Bottke et al., 2005a; O’Brien and Greenberg, 2005; Cibulková et al., 2014) (Fig. 2). This approximation can provide interesting insights; for example, not including the Yarkovsky/resonance “sink” for small bodies may have a substantial affect on the collisional evolution of the main belt, with more projectiles left behind that can disrupt large main-belt asteroids (Cibulková et al., 2014).

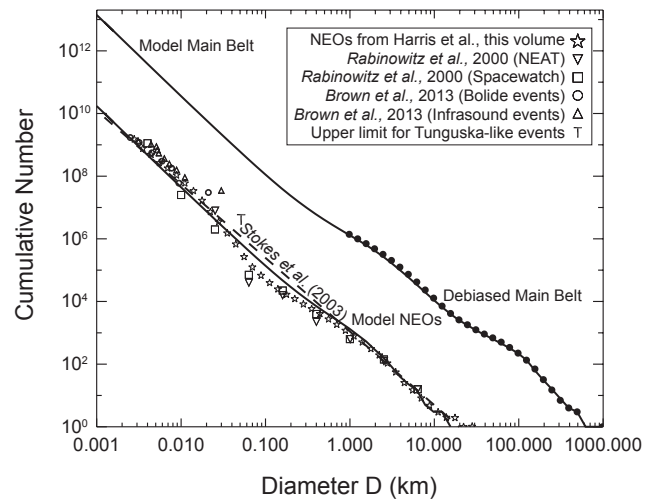


Fig. 2. The estimated present-day main belt and NEO populations according to Bottke et al. (2005b) model runs (solid lines). For reference, we plot our results against an estimate of the NEA population made by Stokes et al. (2003), who assumed the $D < 1$ -km size distribution was a power-law extension of the $D > 1$ -km size distribution, and a population discussed in the chapter by Harris et al. in this volume. Our model main-belt population provides a good match to the observed main belt (solid black dots). Most diameter $D \leq 100$ -km bodies are fragments (or fragments of fragments) derived from a limited number of $D \geq 100$ -km breakups (Bottke et al., 2005a). Our NEA model population is compared to estimates derived from telescopic surveys (Rabinowitz et al., 2000), as well as satellite and infrasound detections of bolide detonations in Earth’s atmosphere (Brown et al., 2013). For reference, we also include an upper limit estimate of 50-m NEAs based on the airblast explosion that occurred over Tunguska, Siberia, in 1908. A mismatch between the NEA model and data is seen near $D \sim 0.1$ km.

2.5. Asteroid Disruption by YORP Torques

The Yarkovsky-O’Keefe-Radzievskii-Paddack (YORP) effect is a thermal torque that, complemented by a torque produced by scattered sunlight, can modify the spin vectors of small asteroids (see the chapter by Vokrouhlický et al. in this volume). As an asteroid’s obliquity evolves, its orientation can strongly affect a body’s drift rate across the main belt, and therefore how quickly it reaches a resonance that can take it out of the main belt. YORP can also spin asteroids up or down. If the body has substantial unconsolidated material, or is a rubble pile, it must reconfigure itself to adjust to its new rotational angular momentum budget. In certain cases, this can cause the body to shed mass, potentially creating a satellite or an asteroid pair. Many of the latest aspects of the YORP effect are discussed in the chapters by Vokrouhlický et al. and Walsh and Jacobson in this volume.

YORP spinup may be so efficient at causing small asteroids to shed mass that this mechanism may dominate the production and elimination of bodies for $D < 1$ km. This prospect is exciting, and we believe warrants continued

investigation using a wide range of models in the future. Indeed, recent main-belt modeling work that included collisional disruption and YORP mass-shedding mechanisms show the latter could explain the shape of the main belt SFD for subkilometer- and kilometer-sized bodies (Marzari et al., 2011; Jacobson et al., 2014; see also Penco et al., 2004).

The goal of main-belt collisional models is to include all the major processes that affect mass loss from small bodies — collisions, Yarkovsky-driven removal of bodies, and YORP-driven mass shedding — in a self-consistent manner. So far, the models of Bottke et al. (2005a,b) and Cibulková et al. (2014) include the first two, while the models of Marzari et al. (2011) and Jacobson et al. (2014) include the first and third. Future models will have to include all these effects in the most accurate way possible, with their relative contributions sorted out using constraints. While this sounds straightforward, in practice the modeler must deal with numerous uncertainties, as well as all the feedbacks they produce.

As an example, consider the mismatch between the model and observed SFDs seen in Fig. 2. While a better fit is possible, and it should be a byproduct of the processes above, which one of them, if any, should dominate?

One could argue that varying the Yarkovsky depletion rates of asteroids from the main belt should solve the problem. Unpublished test runs performed by Bottke et al. (2005a,b) have shown that the shape of the main-belt SFD for subkilometer-sized bodies can be reproduced by assuming more asteroids escape over time than previously predicted. The central problem here is that the loss rates of subkilometer-sized bodies from the main belt are highly uncertain, with the coupling between Yarkovsky drift and the frequency/nature of so-called YORP-cycles only modestly well understood at this time (e.g., Bottke et al., 2015a).

Alternatively, the mismatch might be readily fixed by including YORP-driven mass shedding, as suggested by Marzari et al. (2011) and Jacobson et al. (2014). We find this highly plausible, yet there is also much we do not yet understand when it comes to the details of YORP-driven mass shedding (see the chapter by Vokrouhlický et al. in this volume).

Consider that careful explorations of the YORP effect show there is a preference for asteroidal spinup vs. spindown (e.g., Rozitis and Green, 2012; Golubov and Krugly, 2012; Golubov et al., 2014; see also the chapter by Vokrouhlický et al.). With this said, however, spindown must also exist in order to explain the relatively flat spin frequency distribution of small asteroids as well as why numerous very slow rotators exist (e.g., Bottke et al., 2015a). There is also important work that shows that YORP torques are affected by small topographic changes on an asteroid. For example, Statler (2009) used numerical simulations to demonstrate that minor changes in an asteroid's shape, such as the formation of a small crater or even the movement of a boulder from one place to another, could modify the YORP torques enough to change the magnitude and sign of the spin rate. These changes produce a random walk in an asteroid's spin rate,

and has been coined the “stochastic YORP” effect. While more work is needed, stochastic YORP may prevent some small asteroids from undergoing mass shedding as often as predicted (Cotto-Figueroa, 2013; Cotto-Figueroa et al., 2015; Bottke et al., 2015a). This may explain why some small asteroids have shapes that suggest they have largely avoided substantial mass-shedding events. Conversely, certain bodies may return again and again to spinup-driven mass shedding, which may rapidly turn them into top-like shapes (see the chapter by Walsh and Jacobson in this volume). Probing the asteroidal shape dichotomy using numerical modeling work is an intriguing project for the future.

In the end, all these Yarkovsky and YORP-related issues will need to be better explored and quantified if we are to formulate superior main-belt-evolution models in the future.

2.6. Additional Processes

Some processes that affect planetesimal and planet formation have yet to be implemented into main-belt collisional evolution models. Key examples include (1) the implications of hit-and-run collisions, defined as the disruption and escape of portions of large projectiles striking still larger bodies (see the chapters by Scott et al. and Asphaug et al. in this volume); (2) planetesimal collisional evolution taking place side by side with accretion onto protoplanets/planetary embryos with all the appropriate dynamics and fragmentation events modeled correctly (e.g., Levison et al., 2015a,b); (3) the effects of collisions on the dynamical evolution of an asteroid or planetesimal; and (4) the bombardment of main-belt asteroids by planetesimals forming and evolving within the terrestrial planet and gas giant regions (e.g., see the chapters by Morbidelli et al. and Scott et al. in this volume).

Some of these processes are difficult to include in a model until their effects have been evaluated, although they are almost certainly important for particular issues [e.g., hit-and-run collisions may explain the exposed core-like nature of (16) Psyche and (212) Kleopatra; see the chapters by Asphaug et al. and Scott et al. in this volume]. For other processes, their importance is still unclear because planet-formation models are incomplete and/or are lacking in key constraints (e.g., how much net collisional evolution is produced on indigenous main-belt asteroids via planetesimals from the terrestrial planet region?). We believe an exploration of processes (1)–(4) discussed above and their inclusion in future models will greatly improve the state of the art.

3. CONSTRAINTS ON COLLISIONAL-EVOLUTION MODELS

Given the large number of “knobs” that exist in collisional-evolution models, and the fact that these codes may provide the user with non-unique solutions, it is imperative to test results against as many constraints as possible. Given the breadth of predictions for such codes, this means accounting for how individual asteroids, asteroid families, and different asteroid populations have taken on their current

status. With sufficient constraints, bad parameter choices can be eliminated from contention.

On the other hand, it is important that one recognizes that our understanding of main-belt evolution is still limited, and the inclusion of faulty constraints into a code can also produce inaccurate results and poor predictions. Accordingly, most constraints should be treated with some caution, with the modeler and interpreter cognizant that both data and interpretation can and often do change with time.

With these caveats, we present a list of many of the constraints that should be considered when modeling the collisional evolution of the main belt.

3.1. Wavy Main-Belt Size-Frequency Distribution

One of the primary constraints for collisional-evolution models comes from the main-belt SFD. Improved estimates since the review chapter of *Jedicke et al. (2002)* were provided by pencil-beam studies of the main-belt population (*Gladman et al., 2009*), the addition of asteroids colors from the Sloan Digital Sky Survey (SDSS) (e.g., *Parker et al., 2008*), and new infrared data of many main-belt asteroids (see the chapters by *Mainzer et al.* and *Masiero et al.* in this volume). The inclusion of all these datasets into a single debiased SFD, however, has yet to be attempted, and it is beyond the scope of this chapter.

For basic purposes, one can derive an approximate main-belt SFD using the absolute magnitude H distribution provided by *Jedicke et al. (2002)*, who combined results from the Sloan Digital Sky Survey (SDSS) for $H > 12$ (*Ivezić et al., 2001*) with the set of known main-belt asteroids with $H < 12$. To transform the H distribution into a size distribution, one can use the relationship between asteroid diameter D , absolute magnitude H , and visual geometric albedo p_v provided by *Fowler and Chillemi (1992)*

$$D = \frac{1329}{\sqrt{p_v}} 10^{-H/5} \quad (8)$$

A model main-belt SFD was made by *Botke et al. (2005a)*, who set p_v to 0.092 in order to match the observed asteroids described cited in *Farinella and Davis (1992)*. This population is shown in Fig. 2. Overall, the observed and debiased main-belt SFD is wavy, with “bumps” near $D \sim 3$ km and one near $D \sim 100$ km. The reason for these bumps will be discussed in section 4.

For more precise constraints, and more model variables, one can treat different regions of the main belt separately. For example, *Cibulková et al. (2014)* divided the main-belt population into six distinct components: inner, middle, pristine, outer, Cybele, and high-inclination regions. This allowed them to track how each different regional SFD evolved in response to various collisional and dynamical processes. The observed SFDs in each region, however, have yet to be debiased, which means they must be treated as lower limits for modeling constraints.

3.2. Asteroid Families

Asteroid families provide another powerful way to constrain asteroid collisional models. As discussed in the chapter by *Nesvorný et al.* in this volume, these remnants of cratering and catastrophic disruption events are identified in the main belt by their clustered values of proper semimajor axes a_p , eccentricities e_p , and inclinations i_p . The problem with using them to test our model runs is that estimates of ancient family ages can be imprecise and small families can also be eliminated over time by collisional and dynamical processes.

For this reason, the best starting constraints come from families where the parent body was large enough that their fragments could not be erased over 4 G.y. of evolution. We assume families formed prior to 4 G.y. ago were erased by sweeping/jumping resonances produced by late giant planet migration (see the chapter by *Morbidelli et al.* in this volume). Using results discussed in *Durda et al. (2007)* (see also *Cibulková et al., 2014*), there are approximately 20 observed families created by catastrophic disruptions of parent bodies with sizes $D_{PB} > 100$ km, where the ratio of the largest fragment’s mass to the parent body mass is $M_{LR}/M_{PB} < 0.5$ (Fig. 3).

It is also useful to use the distribution of family parent body sizes to compare model to data. In one case, *Botke et al. (2005a,b)* used results later published in *Durda et al. (2007)* to argue that the number of families formed over the last 3.5 G.y. from catastrophic breakups of parent bodies whose sizes were within incremental logarithmic-separated bins centered on diameters $D = 123.5, 155.5, 195.7, 246.4, 310.2, \text{ and } 390.5$ km were 5, 5, 5, 1, 1, 1, respectively. New family identifications discussed in the chapter by *Nesvorný et al.* in this volume can be used to update these values.

Ideally, a good collisional model must account for all types of collisions, even relatively small cratering events. For the purpose of comparison with observations, one has to carefully select synthetic events that would still be observable. Even

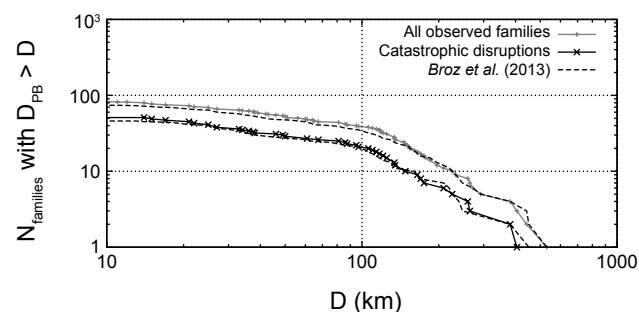


Fig. 3. A production function [i.e., the cumulative number $N(>D)$ of families with parent-body size D_{PB} larger than D] for all observed families (gray) and families corresponding to catastrophic disruptions (black), i.e., with largest remnant/parent body mass ratio lower than 0.5. Adapted from *Brož et al. (2013)* and updated according to the chapter by *Nesvorný et al.* in this volume. The families were assumed to form prior to 4 G.y. ago (see Fig. 4).

though this number ($N_{\text{fam}} \sim 20$) appears well defined above, it is difficult to assess its uncertainty for the following reasons:

- Determining the size of the parent of an asteroid family depends on the observed fragment distribution, which has experienced collisional and dynamical evolution, and the nature of the precise breakup involved, which may be uncertain. The existence of interlopers within the family can also be hard to exclude.
- There are overlapping families that are difficult to separate unambiguously [e.g., several families exist in the Nysa/Polana region (M. Dykhuis, personal communication)].
- The method used for the parent body size determination in *Durda et al. (2007)* may exhibit some systematic issues since it involves a number of assumptions.

Taken together, the uncertainty of N_{fam} is at least the order of a few, if not more.

The distribution of the dynamical ages and sizes of families, as derived using the methods discussed in the chapter by Nesvorný et al. in this volume, may also provide another metric to estimate family completeness. For example, Fig. 4 shows estimates of the ages of cratering and catastrophic disruption events for families derived from different parent body sizes (*Brož et al., 2013*). We caution the reader that discerning these values for heavily evolved ancient families is problematic, and large uncertainties exist. We therefore use Fig. 4 as a guide to glean insights into interesting possibilities, not as the last word on this topic.

We focus here on asteroid families with parent body diameters $D_{\text{PB}} > 100$ km; they are presumably more difficult to eliminate by collisional and dynamical processes. For families formed over the last 2 G.y., we find several with $100 < D_{\text{PB}} < 200$ km and few with $D_{\text{PB}} > 200$ km. The opposite is found for families older than 2 G.y.; only a few $100 < D_{\text{PB}} < 200$ -km families exist, while several $D_{\text{PB}} > 200$ km are found.

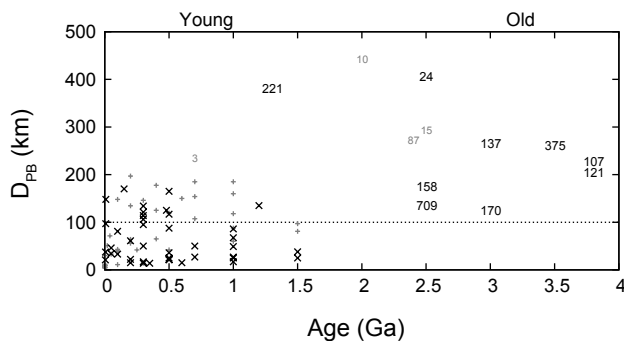


Fig. 4. The relationship between dynamical ages of families and the sizes of their parent bodies. Black labels, shown as x's and numbers, correspond to catastrophic disruptions, while cratering events, shown as crosses and numbers, are labeled in gray. Some of the families are denoted by the designation of the largest member. Adapted from *Brož et al. (2013)* and updated according to the chapter by Nesvorný et al. in this volume.

The difference between the two sets warrants additional study, but statistics of small numbers prevents us from saying they are highly unusual. The probability that two $D_{\text{PB}} > 200$ -km families formed in the last 2 G.y. out of the seven identified with ages < 4 G.y. is 23%. The number of $100 < D_{\text{PB}} < 200$ -km families that formed at different times are also not unusual from a statistical standpoint. Overall, there are also approximately the same number of young ($t_{\text{age}} < 2$ G.y.) and old (> 2 G.y.) families produced by the catastrophic disruptions of $D_{\text{PB}} > 100$ -km bodies.

The most intriguing issue here is that there are no identified $D_{\text{PB}} < 100$ -km families that are > 2 G.y. old. This hints at the possibility that some $100 < D_{\text{PB}} < 200$ -km families older than 2 G.y. are so evolved that they escaped detection. If true, one could argue that something interesting was going on that was producing $D_{\text{PB}} > 100$ -km families in the billion years or so after the completion of the major dynamical depletion events > 4 G.y. (see section 1 and the chapter by Morbidelli et al. in this volume.).

Along these lines, one way to account for the unusual distribution of families in Fig. 4 is to assume that some small families are actually remnants, or “ghosts,” of much larger older families. A possible example might be the cluster of asteroids near asteroid (918) Itha (*Brož et al., 2013*). It exhibits a very shallow SFD, which could be a possible outcome of comminution and dynamical evolution by the size-dependent Yarkovsky effect. An excellent place to look for ghost families would be the narrow portion of the main belt with semimajor axis a between 2.835 and 2.955 AU. This pristine zone, which is bounded by the 5:2 and 7:3 mean-motion resonances with Jupiter, has a limited background population of small asteroids. We postulate it could resemble what the primordial main belt looked like prior to the creation of many big families.

An independent calibration of collisional models might also be based on very *young* families, namely younger (and larger) than some carefully estimated upper limit for which the respective sample is complete. Indeed, there are many examples of young families with well-determined ages: Veritas (8.3 ± 0.5 m.y. (*Nesvorný et al., 2003*), Karin (5.8 ± 0.2 m.y. (*Nesvorný and Bottke, 2004*), Lorre (1.9 ± 0.3 m.y. (*Novaković et al., 2012*), P/2012 F5 (Gibbs) (1.5 ± 0.1 m.y. (*Novaković et al., 2014*), etc. A collisional model then would have to reproduce the number of these events in the last ≈ 10 m.y. or so of the simulation.

3.3. Impact Basins on (4) Vesta

(4) Vesta is one of the most unique asteroids in the main belt. Not only is it among the largest asteroids, with a diameter of 525 km, but it is also has a largely intact basaltic crust that was put in place shortly after it differentiated some 2–3 m.y. after CAIs (see the chapter by Russell et al. in this volume). Decades of groundbased observations, combined with *in situ* observations of Vesta by the Dawn spacecraft, have shown that the spectral signatures found in Vesta's crust are a good match to the howardite, eucrite, and diogenite

(HED) meteorite classes (see the chapter by Russell et al.). We do not consider the impact record on Vesta prior to the formation of this crust, although Vesta's abundance of highly siderophile elements may eventually allow us to infer what happened during this ancient period (e.g., Dale et al., 2012).

Vesta also has two enormous basins that dominate its southern hemisphere: Rheasilvia, a 505-km-diameter crater with an estimated crater retention age of 1 G.y., and Veneneia, a 395-km-diameter crater with a crater retention age of >2 G.y. (Marchi et al., 2012). Rheasilvia, being younger, overlaps with and has largely obscured Veneneia (Schenk et al., 2012; Jaumann et al., 2012). The formation of each basin is also thought to have produced a set of fracture-like troughs, or graben, near Vesta's equator (Buczkowski et al., 2012). Studies of each trough group show they form planes that are orthogonal to the basin centers. Recent simulations of the formation of the Veneneia and Rheasilvia basins using numerical hydrocodes suggest they were created by the impact of 60–70-km-diameter projectiles hitting Vesta near 5 km s^{-1} (Jutzi et al., 2013; see the chapters by Asphaug et al. and Jutzi et al. in this volume). These same events likely produced the majority of the observed Vesta family, a spread out swarm of $D < 10$ -km asteroids in the inner main belt with inclinations and spectral properties similar to Vesta itself (see the chapter by Scott et al. in this volume).

Vesta shows no obvious signs that basins similar in size to Rheasilvia or Veneneia were ever erased or buried after its basaltic crust was emplaced; nothing notable is detected in Vesta's topography, and there are no unaccounted sets of troughs that could be linked with a missing or erased basin. This means Vesta is probably complete in Rheasilvia- or Veneneia-sized basins. This constrains both the size of many primordial populations as well as how long they could have lasted on Vesta-crossing orbits (e.g., main-belt asteroids, leftover planetesimals from terrestrial and giant planet formation, the putative late heavy bombardment (LHB) population, Jupiter-family comets, etc.).

As a working example, consider that if we use the main-belt asteroid population described in Bottke et al. (1994), where there are 682 main-belt asteroids with $D > 50$ km, we find that the probability that Vesta has 0, 1, 2, or 3+ Rheasilvia/Veneneia formation events over the last 4 G.y. is 50%, 35%, 12%, and 3%, respectively. If Rheasilvia and Veneneia are actually both <2 G.y. old, however, these values change to 70%, 25%, 4%, and 0.5%, respectively. The 4% probability for the observed situation is surprisingly small, and it suggests two possibilities: Veneneia's crater retention age was strongly affected by the Rheasilvia formation event, and its formation age is older than its crater retention age (Schenk et al., 2012), or the basins on Vesta's surface beat the odds. Note that testing modestly smaller projectiles to make the basins, such as $D > 35$ -km asteroids (Asphaug et al., 1997), only increases the probabilities above by a factor of 2 or so.

These calculations become even more interesting if we assume the main-belt population was larger in its early history, and/or that it was hit by objects from outside the main

belt (see the chapter by Morbidelli et al. in this volume). Bottke et al. (2005a) argued the main belt experienced the equivalent of ~ 7.5 – 9.5 G.y. of collisional evolution over the last 4.56 G.y. (i.e., roughly translated as the number of impacts Vesta would get if it resided in the current main-belt population for this time; see section 4). For simplicity, we round this value to 10 G.y., which makes the probability of getting 0, 1, 2, or 3+ basins at any time in Vesta's history 17%, 30%, 27%, and 20%, respectively. This would place the Rheasilvia/Veneneia combination near the center of the probability distribution. If Rheasilvia/Veneneia formed <2 G.y. ago, however, we not only have to explain their existence, but also the absence of ancient basins; large primordial populations are more likely to create ancient basins than young ones. The probability of these events taking place is only $\sim 1\%$.

Therefore, from a purely statistical point of view, one could argue that the main belt was probably more massive in the past, and that Veneneia's minimum age of ~ 2 G.y. is not its formation age. An older age for Veneneia would also allow it to be the source for numerous Vesta family members with low inclinations, which need billions of years to reach these orbits via Yarkovsky drift and resonances (Nesvorný et al., 2008). Further work will be needed to see if the “facts on the ground” confirm or reject these predictions.

3.4. Near-Earth Asteroids, Asteroid Craters, and Lunar Craters

Asteroids in the main belt have struck other asteroids throughout the lifetime of the solar system. This means that projectile SFDs ranging from a few meters to multi-kilometer sizes can be constrained over hundreds of millions to billions of years by craters found on asteroids imaged by spacecraft missions (see the chapter by Marchi et al. in this volume). The main-belt SFD also produces planet-crossing asteroids via the combined Yarkovsky/YORP effects (see the chapter by Vokrouhlický et al.). This means that the observed planet-crossing asteroid population can also be used to provide main-belt SFD constraints. We focus here on the best-understood component of the population, namely the NEAs (see the chapter by Harris et al.). Finally, Earth-crossing asteroids in the NEA population have slammed into Earth and the Moon over billions of years, which means the crater SFDs and impact byproducts on these worlds can help us determine how the main-belt SFDs have evolved over these times.

The key issue for all these data is interpretation; the ages and SFDs of cratered terrains are often uncertain or complicated, and short-term changes in the flux or shape of impacting SFDs can be hard to decipher amid the integrated histories of cratered surfaces. For this reason, a full discussion of all cratering issues is beyond the scope of this section. Instead, we provide a brief summary of how asteroid and lunar craters, together with the debiased NEA population, can be used as constraints for main-belt collisional models, provided appropriate caution is employed by the reader.

The crater histories of the asteroids visited by spacecraft are reviewed in the chapters by Marchi et al. and Barucci et al. in this volume. They found that the crater SFDs that do the best job of showing off the main-belt production population are found on (951) Gaspra and (4) Vesta. Crater data for Vesta is shown in Fig. 5, while Gaspra crater data can be found in the chapter by Marchi et al. The cumulative crater SFD found on or near Vesta's Rheasilvia basin shows, from large to small craters, a wavy shape: a steep slope up to an inflection point at 20 km, a shallow slope to a roundoff near 4 km, an even shallower slope to 0.8 km, and a steep slope to 0.01 km, where the resolution limit is reached. The craters superposed on Vesta's Marcia crater and on Gaspra's surface have the same slope as that found on Rheasilvia for <0.8-km craters. If we assume the scaling relationship between asteroids and craters is a simple factor of 10 (Bottke and Chapman, 2006; Marchi et al., 2013), these values yield a wavy asteroid SFD with inflection points at ~2 km, 0.4 km, and 0.08 km. As a caveat, it is also possible that some aspects of the wavy crater SFD on Vesta are a byproduct of terrain properties (Marchi et al., 2012, 2014).

The nature of the NEA SFD is thoroughly discussed in this volume in the chapter by Harris et al., so we only discuss a few aspects of it here. Their best estimate of the NEA population is shown in Fig. 2. Its wavy shape is broadly similar to a scaled version of the crater SFD found on Vesta in Fig. 5,

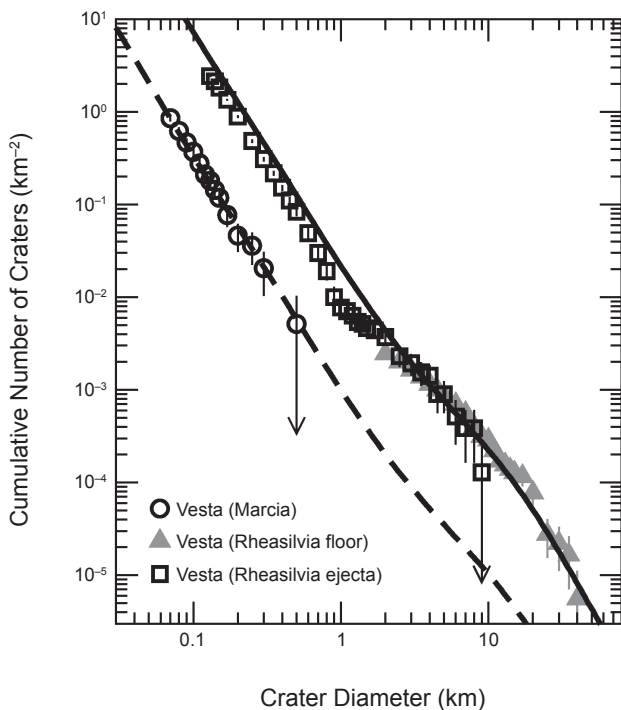


Fig. 5. The crater SFDs found on the young terrains of Marcia crater and the floor and ejecta blanket of the basin Rheasilvia. Details can be found in the chapter by Marchi et al. in this volume. The dashed lines are the estimated main-belt production function derived using the results of Bottke et al. (2005a,b). The fit is good except near $0.7 < D < 2$ km, where the model steepens too quickly.

although some differences exist; recall that the main-belt SFD is modified en route to the NEA population by Yarkovsky/YORP-driven asteroid migration (e.g., Morbidelli and Vokrouhlický, 2003). The inflection points for the NEA population in Fig. 2, however, are at approximately the same sizes as derived above: ~2, 0.4, and 0.1 km. Our interpretation is that the broad shapes of the main-belt and NEA population have not been strongly modified for an extended period.

A similar analysis can be performed on the lunar crater SFD plotted in Fig. 1 of Ivanov et al. (2002). The broad shapes are the same as that above, with crater diameter inflection points at 64 km, 1.4 km, and 0.3 km. The middle inflection point at 1.4 km possibly straddles a slowly bending region between 1 and 3.5 km. Using crater-scaling-law relationships from Melosh (1989), these values roughly correspond to 2–3 km, 0.03–0.16 km, and 0.009–0.014 km. As before, these compare well to the values above.

In summary, the scaled asteroid and lunar crater data, together with the NEA population, all suggest a wavy main-belt SFD with inflection points near ~2–3, 0.4, and 0.1 km. Collectively, these results imply that the shape of the main-belt SFD for asteroid sizes smaller than 5–10 km has not substantially changed for billions of years.

If the shape of the main-belt SFD has remained the same over time, what can be said about the size of the population? Here we turn once again to the Moon, our benchmark for solar system chronology. Many nearside lunar terrains have been dated by returned samples. The crater populations found on these surfaces give us a sense of how the Earth-crossing impactor flux has changed with time (e.g., Stöffler and Ryder, 2001; Morbidelli et al., 2012). Given that this flux is fed by the main-belt population, changes in the lunar impactor flux over time should correspond at some level to what took place in particular regions of the main belt.

Studies of small lunar craters ($D < 1$ km) on specific Copernican and Eratosthenian-era terrains suggest the impact flux of very small impactors has been fairly constant, within a factor of 2 or so, for the last 3.2 G.y. (e.g., Ivanov et al., 2002; Marchi et al., 2009; Hiesinger et al., 2012; but see also Robbins, 2014). For reference, the ages of the former era are often considered to be roughly 1 G.y. old, while those of the latter are defined by the ages of samples returned by the Apollo 12 astronauts (Stöffler and Ryder, 2001). This implies the main-belt population in the inner and central main belt feeding $D < 0.05$ -km bodies to resonances may have been reasonably stable as well.

For larger impactors, the lunar data is more difficult to interpret, although it also hints at a steady state flux. For example, the best available crater SFD of the largest Copernican- and Copernican and Eratosthenian-era craters on the Moon are shown in Fig. 6 (McEwen et al., 1997; Ivanov et al., 2002). The Copernican and Eratosthenian-era craters are roughly a factor of 3 higher than the Copernican-era craters. If the ages of these eras suggested above are reasonable, these data would indicate there have been a fairly steady supply of kilometer-sized main-belt asteroids to the NEA population and the Moon over 3 G.y. (to a factor of 2 or so).

We caution that this interpretation may be subject to revision in the near future once data from the Lunar Reconnaissance Orbiter has been fully evaluated (e.g., Kirchoff et al., 2013; Robbins, 2014). For example, asteroid-family-forming events in strategic locations could potentially affect the lunar impact flux for some period of time (Nesvorný et al., 2002; Bottke et al., 2007, 2015). Given our present state of knowledge, however, it is fair to say that deviations from a steady state over long time spans may be modest for most projectile sizes.

There are two main reasons these results are of critical importance for collision models:

1. Collisional models of the main-belt and NEA SFD need to achieve a quasi-steady-state for the last several billions of years (or have an alternative way to explain the above constraints). This likely rules out scenarios where a very large main-belt SFD is ground down over billions of years of comminution, with the observed SFD only achieved near the present time (see Davis et al., 2002). Such models should produce strongly decaying lunar impact fluxes over the last 3 G.y., and they are not observed.

2. A steady-state main-belt SFD allows modelers to predict the ages of asteroid surfaces with reasonable accuracy, although caution should still be employed (see the chapter by Marchi et al. in this volume).

3.5. Main-Belt Binaries Formed by Impacts

The population of certain types of asteroid binaries may also constrain the collisional evolution of the main belt. Using numerical hydrocode simulations to model asteroid impacts on $D = 100$ -km target bodies, Durda et al. (2004) found that large-scale cratering events can create fragments whose trajectories can be changed by particle-particle interactions and by the reaccretion of material onto the remnant target body. Under the right circumstances, impact debris can enter into orbit around the remnant target body, which is a gravitationally reaccreted rubble pile, to form a SMAShed Target Satellite (SMATS).

Here we only discuss SMATS made by subcatastrophic collisions. We expect those SMATS to be rather isolated in space; while their formation events produce asteroid families dominated by small fragments, most of these bodies are readily removed or dispersed by collisional and dynamical evolution. As of a few years ago, detection limits of groundbased adaptive optics searches limited the discovery of SMATS to primary-to-secondary diameter ratios smaller than 25 (e.g., Merline et al., 2002). This population is thought to be complete, so we focus on these binaries here. In a survey of 300 large main-belt asteroids, Merline et al. (2002) reported four $D > 140$ -km bodies that had relatively large satellites (i.e., $D > 10$ km) that were not in asteroid families produced by catastrophic disruption events: (22) Kalliope, (45) Eugenia, (87) Sylvia, and (762) Pulcova.

Additions since that time to the SMATS record could include (216) Kleopatra and (283) Emma, whose primaries have diameters that are nearly 140 km. The secondary

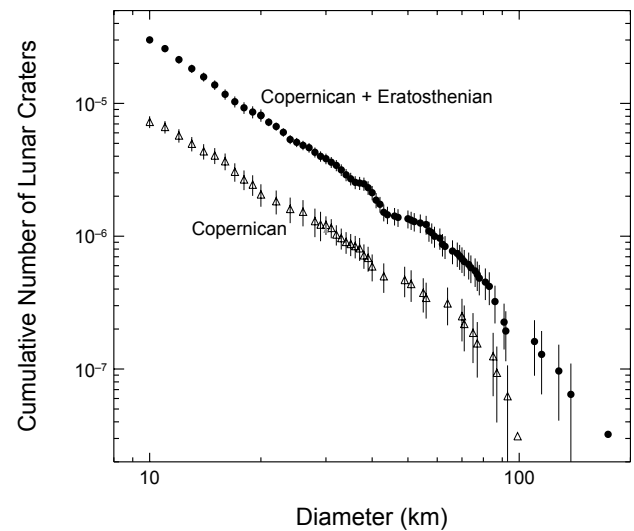


Fig. 6. Lunar craters in the Copernican and Copernican and Eratosthenian eras as defined by Wilhelms et al. (1978) and McEwen et al. (1997). The absolute ages of these craters are often considered <1 and <3.2 G.y. old (Stöffler and Ryder 2001), although the age of the former is debated (e.g., Ryder et al., 1991). The plotted Copernican-era craters are a combination of nearside craters (Wilhelms, 1987) and far-side rayed craters (McEwen et al., 1997). These estimates may be revised using Lunar Reconnaissance Orbiter data in the near future.

sizes of Eugenia and Emma, however, are very close to our primary-to-secondary diameter ratio limit, and Kleopatra appears to have an iron rather than stony composition, such that the results of Durda et al. (2004) may not be applicable. This leaves the net value somewhere in the range of 3–6. The binary (90) Antiope is excluded here because it is a likely byproduct of the catastrophic disruption that produced the Themis family.

Using their runs, Durda et al. (2004) estimated that the expected frequency of SMATS-forming events by non-catastrophic collisions in the present-day main belt was $f = 0.9\text{--}1.7 \times 10^{-11} \text{ yr}^{-1}$. If one then assumes that the current population of $D > 140$ -km bodies, $N = 94$, is similar to that from 4 G.y. ago, we would expect these production rates to yield 3–6 SMATS on average. These results are an excellent match to the 3–6 SMATS discussed above.

These results place upper limits on what happened during the primordial phase of the asteroid belt, depending on the planet formation evolution model invoked. For example, as described in the chapter by Morbidelli et al. in this volume, the main belt potentially had an early massive phase, where numerous SMATS should have been made. A dynamical depletion event at the end of this phase would then remove most of the excess mass as well as most of the newly formed SMATS. Effectively, this would make the remnant number of primordial SMATS the product of f , N , and the time interval that the excess population existed in the main belt. For Nice model simulations (see the chapter by Morbidelli et al.),

where the main belt is only a few times more massive than the current population for ~ 0.5 G.y., this would yield ~ 1 extra SMAT on average, not enough to affect the results above.

On the other hand, SMATS provide powerful constraints against evolution scenarios where collision grinding alone removes most of the primordial mass of the main belt. This scenario is already problematic, as discussed above, but numerous collisions may produce a net amount of SMATS that exceeds observations. Similarly, massive planetesimal populations on terrestrial planet-crossing orbits may create numerous SMATS. Given that we see little evidence for an abundance of primordial SMATS, these models can potentially be tested on this basis.

3.6. Asteroid Spin Rates and Spin States

Asteroid spin rates are affected by collisions, so it is plausible they can be used as constraints on main-belt evolution. A problem with this is that many $D > 50$ – 100 -km bodies may still have spins that were largely put in place by the planetesimal accretion process. A review of the spin rate literature for the largest asteroids can be found in *Bottke et al.* (2005a). For smaller bodies, the spin rates and obliquities of $D < 30$ – 40 -km asteroids are likely dominated by the effects of YORP thermal torques (e.g., *Pravec et al.*, 2002; see the chapter by *Vokrouhlický et al.* in this volume). Given this, an unambiguous signal of collisions affecting spin vectors in the main belt may be limited to bodies whose evolutionary context is well understood.

The interested reader can consider the spin-evolution models of *Farinella et al.* (1992) and *Marzari et al.* (2011) for their views on this topic. They should also examine results from the numerical hydrocode simulations of *Love and Ahrens* (1997), who argued that small erosive collisions have a minimal effect on an object's spin, while catastrophic disruption events essentially destroy all "memory" of the target body's initial spin. The collisional signal we are looking for, therefore, may be limited to specific remnants of certain family-forming events.

An alternative way to obtain a model constraint may be found in the spin vectors of asteroids in the Koronis asteroid family. The Koronis family is thought to be one of the asteroid belt's most ancient families, with an estimate age of 2–3 G.y. (see the chapter by *Nesvorný et al.* in this volume). After years of painstaking observations of Koronis family members, including 21 of the 25 brightest Koronis family members, *Slivan et al.* (2003, 2009), *Slivan* (2002), and *Slivan and Molnar* (2012) reported that nearly all of the observed 15–40-km-diameter Koronis family members with prograde spins have clustered spin periods between 7.5 and 9.5 h and spin obliquities between 39° and 56° . Those with retrograde spins have obliquities larger than nearly 140° with periods either < 5 h or > 13 h. *Vokrouhlický et al.* (2003) demonstrated that all these spin states were a byproduct of YORP thermal torques. The prograde cluster was created by an interaction between YORP torques and spin orbit resonances, and are now called "Slivan states."

The predicted timescales for these objects to reach these spin states is several billions of years. During that time, collisions did not strongly affect their spin periods or their obliquities; if they had, we would see at least a few bodies with random spin vector values. Limits on this come from (243) Ida, a member of the prograde cluster with dimensions of $53.6 \times 24.0 \times 15.2$ km; it was apparently unaffected by the formation of two ~ 10 -km-diameter craters formed on its surface.

Statistically, we would expect catastrophic disruptions to be more rare than smaller, less-energetic impact events that can modify an asteroid's spin state. In the ancient Koronis family, however, the spin vectors of many large objects show no evidence that collisions have affected them. This presents a key challenge to collisional models that assume disruption events among 20–40-km bodies are relatively common; can this outcome be reconciled with the spin states of Koronis family members? A similar argument could potentially be developed regarding the anisotropic obliquities found among $D < 30$ -km asteroids residing in the background main-belt population (e.g., *Hanus et al.*, 2013).

3.7. Additional Constraints

The constraints discussed above are far from complete, and many other datasets could be brought to bear in a collisional model. For space reasons, we do not include a discussion of (1) the cosmic-ray-exposure ages of stony meteorites (e.g., *Eugster*, 2003); (2) the orbital distribution of fireballs (e.g., *Morbidelli and Gladman*, 1998); (3) the population of V-type asteroids across the main belt (see the chapter by *Scott et al.* in this volume); (4) the crater records found on Mercury, Venus, Earth, and Mars (e.g., *Ivanov et al.*, 2002); (5) all asteroid families not discussed here (see the chapter by *Nesvorný et al.* in this volume); and (6) the shock degassing ages of meteorites (e.g., *Marchi et al.*, 2013). In fact, the subject of collisional evolution in the main belt is rich enough that data from numerous *Asteroids IV* chapters could probably be employed as well.

4. INSIGHTS FROM MODELING RESULTS

Existing collisional modeling work has provided us with insights into the nature of planetesimal formation, asteroid fragmentation and evolution, planet-formation processes, and the bombardment history of the inner solar system. Here we summarize some of those findings.

4.1. The Relationship Between the Main-Belt Size-Frequency Distribution and Asteroid Disruption Scaling Laws

The bump in the main-belt SFD near $D \sim 2$ – 3 km (Fig. 2) is a byproduct of collisional evolution (*Campo Bagatin et al.*, 1994; see *Davis et al.*, 2002), and is driven by a change in the Q_D^* function near $D \sim 0.2$ km. To trace its origin, we start with the classic work of *Dohnanyi* (1969) (later

expanded by *Williams and Wetherill, 1994*, and *Tanaka et al., 1996*), who analytically modeled collisions among a SFD of self-similar bodies and found the steady-state SFD should follow a differential power law with an exponent of -3.5 . Dohnanyi assumed that the strength per unit mass of the colliding bodies is independent of size. In reality, though, for bodies smaller than ~ 0.2 km in diameter, material properties cause strength to decrease with increasing size, while for larger bodies, self-gravity makes it more difficult to shatter a body and disperse its fragments, leading to an increase in strength with increasing size (e.g., *Asphaug et al., 2002; Holsapple et al., 2002; Davis et al., 2002*). This provides us with the classic Q_D^* function discussed above.

The dependence of the power-law index of the size distribution on these parameters was explored analytically by *O'Brien and Greenberg (2003)*, and we repeat the main results here. First consider the steady-state of a colliding population of bodies whose strength is described by a single power law. The population is described by the power law

$$dN = BD^{-p}dD \quad (9)$$

where dN is the incremental number of bodies in the interval $(D, D + dD)$. While B should technically be negative as there are more small bodies than large bodies, it is defined to be positive here to avoid the physically unrealistic result of having negative numbers of bodies in a given size interval. p is the power-law index of the population. Equation (9) would plot as a line with a slope of $-p$ on a log-log plot.

O'Brien and Greenberg (2003) considered the case where the impact strength Q_D^* is given by a power law

$$Q_D^* = Q_0 D^s \quad (10)$$

where Q_0 is a normalization constant and s is the slope of equation (10) on a log-log plot. They find that, in collisional equilibrium, the power-law index p in equation (9) is given by

$$p = \frac{7 + s/3}{2 + s/3} \quad (11)$$

For $s = 0$, which corresponds to size-independent strength Q_D^* , this gives the classical Dohnanyi steady-state solution of $p = 3.5$. For the more realistic case where Q_D^* decreases with increasing size for small bodies and increases for larger bodies once gravity becomes important (as schematically shown in Fig. 1), *O'Brien and Greenberg (2003)* show that the strength- and gravity-scaled portions of the size distribution have power-law indices p_s and p_g that are only dependent on the slope of Q_D^* in the strength and gravity-scaled regimes s_s and s_g , respectively. The power-law index of the size distribution in the strength-scaled regime p_s has no dependence on the slope s_g of Q_D^* in the gravity-scaled regime, and vice versa; p_s is found by using s_s , and p_g is found by using s_g . Because s_s is usually negative and s_g is usually positive, equation (11) yields $p_s > 3.5$ and $p_g < 3.5$.

While the general slope of the size distribution in the gravity regime is unaffected by Q_D^* in the strength regime,

the transition in slope of the size distribution will lead to waves that propagate through the size distribution in the gravity regime. In the derivation of p_g , it is implicitly assumed that all asteroids were disrupted by projectiles whose numbers were described by the same power law. However, for those targets just larger than the transition diameter D_t between the strength- and gravity-scaled regimes (i.e., near the small end of the gravity-scaled regime), projectiles are mostly smaller than D_t , and hence are governed by the strength-scaled size distribution. As these projectiles will be stronger and hence more numerous than would be expected by assuming that all bodies are gravity-scaled, they will lead to a depletion of bodies of diameter D_t . This underabundance of bodies of diameter D_t (a “valley”) leads to an overabundance of bodies that impactors of diameter D_t are capable of destroying (a “peak”), which in turn leads to another “valley” and so on. This results in a wave that propagates through the large-body size distribution, as can be seen in Fig. 2. The average power-law index p_g of the population in the gravity-scaled regime will not be significantly changed by the initiation of this wave; the wave oscillates about a power law of slope p_g . Analytical expressions for the amplitude of the waves, as well as the approximate positions of the “peaks” and “valleys” in the size distribution, are derived in *O'Brien and Greenberg (2003)*. The waves will not continue on to larger bodies if they have long collisional lifetimes. The origin of the bump for $D > 100$ -km bodies is discussed in the next section.

Finally, we note that removing all small bodies instantaneously from the population (i.e., creating a small body cutoff) can also launch a wave into the size-frequency distribution (*Campo-Bagatin et al., 1994; Penco et al., 2004*). The effect is minimized, however, if removal is more gradual. This was demonstrated by both *O'Brien (2009)*, who found the depletion expected from Yarkovsky removal is too small to significantly perturb the main-belt size distribution (section 2.4), and by *Durda et al. (1997)*, who found the same result when they modeled the expected dust distribution created by the main belt collisions and Poynting-Robertson drag.

4.2. Large Asteroids as Byproducts of Planetesimal Formation

One of the most difficult issues to deal with concerning main-belt evolution is estimating the initial SFD created by planetesimal formation mechanisms. Given the current uncertainties surrounding planet formation, a enormous range of starting SFDs are theoretically plausible. This has caused many groups to winnow these possibilities down using collisional models.

For example, *Bottke et al. (2005a,b)* tested a wide range of initial SFDs and Q_D^* functions to determine which combinations work the best at reproducing the observational constraints discussed in section 3. They found that Q_D^* functions similar to those derived in numerical SPH experiments of asteroid breakup events (*Benz and Asphaug, 1999*)

tended to work the best (Fig. 1), although this made their $D > 100$ -km asteroids very difficult to disrupt. Accordingly, they inferred that the shape of the main-belt SFD for $D > 100$ -km asteroids was probably close to its primordial shape (Fig. 2). Interestingly, this prediction is consistent with several pioneering papers from the 1950s and 1960s (Kuiper *et al.*, 1958; Anders, 1965; Hartmann and Hartmann, 1968).

Next, they tested initial main-belt SFDs where the incremental power law slope of -4.5 between $100 < D < 200$ km had been extended to $D < 100$ -km bodies (Fig. 7). This eliminated the observed bump near $D \sim 100$ km. They found bodies in this size range were so difficult to disrupt that initial SFDs with these shapes could not reproduce constraints. They argued from this that the bump near 100 km in the main-belt SFD is primordial and that $D < 100$ -km bodies probably had a shallow power law slope. Accordingly, this would indicate the planetesimal-formation process favors the creation of bodies near 100 km (or larger), with smaller bodies increasingly fragments produced by the disruption of large asteroids. These results may act as a guide for those studying planetesimal-formation processes (e.g., Morbidelli *et al.*, 2009; see the chapter by Johansen *et al.* in this volume).

4.3. Collisional Evolution of the Primordial Main Belt

To understand the history of the main belt, it is important to quantify how much collisional evolution has taken place there over its history. This means choosing a starting SFD and then evaluating what it takes to reach its present-day

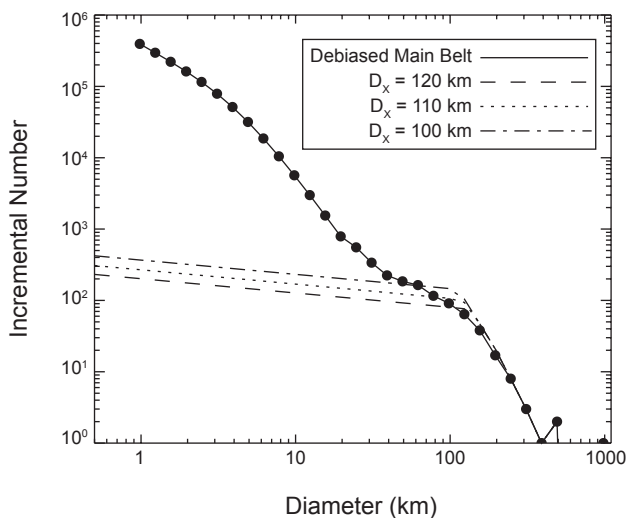


Fig. 7. The debiased main-belt size-frequency distribution as defined in the main text (solid line). The dashed curves show possible initial shapes of the primordial main belt SFD (Bottke *et al.*, 2005a). They found a best fit in their runs for an elbow near $D_x \sim 110$ – 120 km. It is likely that the primordial population was larger than the SFDs shown here, with most of the mass eliminated by dynamical processes.

state. The problem is there are many different ways to get from start to finish, and the available constraints may be insufficient to tell us which pathways are favored.

In order to glean insights into this, one can adopt a simplistic but useful metric that can help us evaluate what different evolutionary paths might do. First, let us assume that the main belt is roughly self-contained in terms of collisions, such that we can largely ignore impacts from external sources like escaped main-belt asteroids, leftover planetesimals, comets, etc. Second, we assume the intrinsic collision probabilities and impact velocities of main-belt asteroids hitting one another have remained unchanged over its history. Third, we assume the main belt’s SFD has been close to its current shape throughout its history, although it may have been larger in the past. We define this size to be a factor f_{MB} , the ratio of the main belt’s SFD during some past interval of time defined as ΔT over the present-day main-belt SFD. Together, these values allow us to estimate the degree of collisional evolution experienced by the main belt in terms of the time exposed to different population sizes.

This metric allows to play with evolution scenarios. The simplest example is the nominal case where the current main-belt SFD ($f_{\text{MB}} = 1$) undergoes collisional evolution over its lifetime ($\Delta T = 4.56$ G.y.). The two values multiplied together yield 4.56 G.y. of collisional grinding. In a more complicated example, we assume a dynamically excited primordial main belt had $f = 300$ for 3 m.y. (0.003 G.y.). At that point, most of the population was lost via escaping embryos or a migrating Jupiter, which reduced it to $f_{\text{MB}} \sim 5$ for ~ 0.5 G.y. Then, at ~ 4 G.y., 80% of the bodies were lost via sweeping resonances driven by late giant planet migration, which left the surviving population close to its current state ($f = 1$) for the next ~ 4 G.y. Taking all of the multiples, one can say that collectively the survivors experienced $(0.9 + 2.5 + 4) = 7.4$ G.y. of collisional evolution. This pseudo-time tells us that this main belt roughly experienced the collisional evolution equivalent of a $f_{\text{MB}} = 1$ main belt going through 7.4 G.y. of comminution.

Using a collisional model that took advantage of these concepts, as well as the constraints above, Bottke *et al.* (2005a) found median pseudo-times of 7.5–9.5 G.y. for their best-fit runs, with error bars of a few million years on each end of this range. An example of one of their runs is shown in Fig. 8. Their interpretation was that the main-belt SFD obtained its wavy shape by going through an early time interval where the main-belt survivors were exposed to many more projectiles than are observed today, with most of those bodies due lost to dynamical processes. Thus, the wavy main-belt SFD could be considered a “fossil” produced in part by early collisional evolution in the primordial main belt.

This pseudo-time range above can be used to explore dynamical-evolution scenarios, particularly those that create abundant main-belt populations. For example, using our simple metric, one could replace the middle component, which roughly corresponds to the “Jumping Jupiter” version of the Nice model (Morbidelli *et al.*, 2010; Marchi *et al.*, 2013; see also Nesvorný, 2011; Nesvorný and Morbidelli, 2012),

with the original Nice model, where $f_{\text{MB}} \sim 20$ for ~ 0.5 G.y. (Gomes et al., 2005). This change yields $(0.9 + 10 + 4) = 14.9$ G.y., a pseudo-time outside the favored range. While it cannot be ruled out statistically, it does suggest that collisional evolution needs to be explored in greater depth here.

Another interesting property of Fig. 8 is that once it achieves the shape of the current main belt's SFD, it tends to keep that shape for an extended time. This would explain why the main-belt SFD could remain in a near-steady-state condition for billions of years. While it would be constantly changing and losing bodies by collisional, dynamical, and

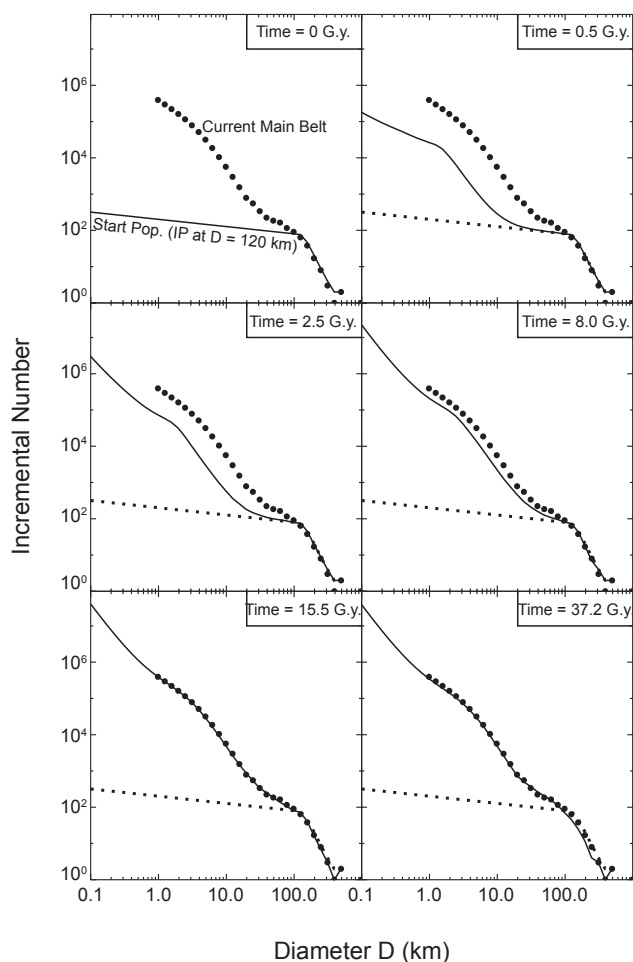


Fig. 8. Six snapshots from a representative run where Bottke et al. (2005a) tracked the collisional evolution of the main-belt size distribution for a pseudo-time of 50 G.y. This run uses a starting population with $D_x = 120$ km. The bump near $D \sim 120$ km is a leftover from accretion, while the bump at smaller sizes is driven by the transition at $D \sim 0.2$ km between strength and gravity scaling regimes in Q_D^* . The model main belt achieves the same approximate shape as the observed population at $t_{\text{pseudo}} = 9.25$ G.y. (not shown). The model closely adheres to the observed population for many gigayears after this time. Eventually, comminution eliminates enough $D > 200$ -km bodies that the model diverges from the observed population.

YORP spinup processes, it would also be steadily replenished by new large breakup events. This means the vast majority of disruption events produce too few fragments to push the main-belt SFD out of equilibrium for very long. This result also explains why the nonsaturated crater populations on Gaspra, Vesta (i.e., the Marcia and Rheasilvia terrains), and the Moon appear to have been hit by a projectile population with a similarly shaped SFD for an extended period (see section 3.4).

4.4. Processes Affecting Small Asteroids

A comparison between the model predictions of Bottke et al. (2005b) and the observed NEO population discussed in the chapter in this volume by Harris et al. (Fig. 2) is intriguing for a different reason (see also O'Brien and Greenberg, 2005). The model does a reasonable job of fitting the observed data for small and larger NEOs, but there is a distinct mismatch near $D \sim 0.1$ km. The same kind of discrepancy is found between the model main belt and small craters on Vesta at the same approximate location when the craters are scaled back to projectiles (see chapter by Marchi et al. in this volume) (Fig. 5).

This difference suggests the model may be missing something (see section 2.5):

1. YORP spinup torques produce such efficient mass shedding as asteroids sizes approach $D \sim 0.1$ km that they can influence the shape of the main-belt SFD (Marzari et al., 2011; Jacobson et al., 2014). This same mechanism, however, would need to shut off for $D < 0.1$ km. The reason why YORP mass shedding approaches termination is unknown, but we can think of several possibilities: (i) the physical nature and/or internal structure of small asteroids may be different from large asteroids, with smaller bodies less likely to be rubble-piles; (ii) small asteroids may be more susceptible to being held together by non-gravitational cohesive forces; or (iii) the thermal properties of the small asteroids are different than those of large asteroids and/or small asteroids become isothermal enough that the YORP mass shedding is less pronounced.

2. The Yarkovsky effect is more efficient at delivering small main belt asteroids to resonances than predicted by Bottke et al. (2005b). As more $D \sim 0.1$ km objects are evacuated from the main-belt population, a steady-state deficit of small bodies may be created in of both the main belt and NEO populations near this size. The reason for this increased delivery efficiency may be related to the YORP shut down discussed above. If YORP becomes less efficient, bodies may become less likely to experience YORP cycles that can cause them to random walk in semimajor axis. In turn, this would enhance their escape rate out of the main belt.

These possibilities illustrate the importance of understanding all the physical processes that affect small bodies in the inner solar system; they feed back in interesting ways, and they may ultimately affect how we interpret the ages of surfaces on both asteroids and the terrestrial planets. We look forward to seeing this investigated in the future.

4.5. Monolithic vs. Rubble-Pile Structures

Recent collisional modeling work by *Cibulková et al.* (2014) has also taken a more sophisticated look at the evolution of six different main-belt regions (Fig. 9): inner, middle, “pristine,” outer, Cybele zone, and high inclination. Their goal was to fit the SFDs and asteroid families formed in all these zones. The observed SFDs in these regions were computed from the available WISE satellite data (*Masiero et al.*, 2011; see the chapter by Mainzer et al. in this volume). They also assumed the bodies were either monolithic asteroids or rubble piles, with the fragment SFDs derived from *Durda et al.* (2007) and *Benavidez et al.* (2012), respectively. Their model also allows for dynamical depletion due to the Yarkovsky effect.

Cibulková et al. (2014) found a number of intriguing results. First, treating all asteroids as weak rubble piles as defined by *Benavidez et al.* (2012) led to SFDs that are too shallow below $D < 10$ km, as well as a factor of 2 more large families produced than are observed. This does not necessarily mean that asteroids are not rubble piles; an alternative would be that their disruption law is close to that derived for monolithic objects. New models of how porous rubble-pile asteroids break up suggest this may be the most likely answer (see the chapter by Jutzi et al. in this volume). Second, *Cibulková et al.* (2014) also found that individual breakups are unlikely to change the SFDs of the regions they investigated because small fragments, while numerous, were

quickly destroyed on a ~ 100 -m.y. timescale. This is consistent with the main belt staying close to an equilibrium state.

Finally, even at the current limit of observational completeness (3 to 6 km, depending on the main belt zone), the frequency of collisions becomes comparable to the dynamical removal of bodies by the Yarkovsky effect and major mean-motion resonances (*Bottke et al.*, 2005a,b) or rotational disruption induced by the YORP effect (*Jacobsen et al.*, 2005b) or those in *Cibulková et al.* (2014) seem to be compatible with observations, namely the observed SFDs of main-belt asteroids and NEAs. The same may also be true for the latter process, although this will need to be examined in greater detail with the implications of *Statler* (2009) included. At this time, it is not clear which process dominates.

4.6. Connections Between Asteroid Families and Meteorites

One of the most perplexing issues involving meteorite delivery concerns the fact that we currently have many tens of thousands of meteorites in worldwide collections, yet this population could represent as few as ~ 100 different asteroid parent bodies: ~ 27 chondritic, ~ 2 primitive achondritic, ~ 6 differentiated achondritic, ~ 4 stony-iron, ~ 10 iron groups, and ~ 50 ungrouped irons (e.g., *Burbine et al.*, 2002). If we remove the stony-iron, iron, and differentiated meteorites,

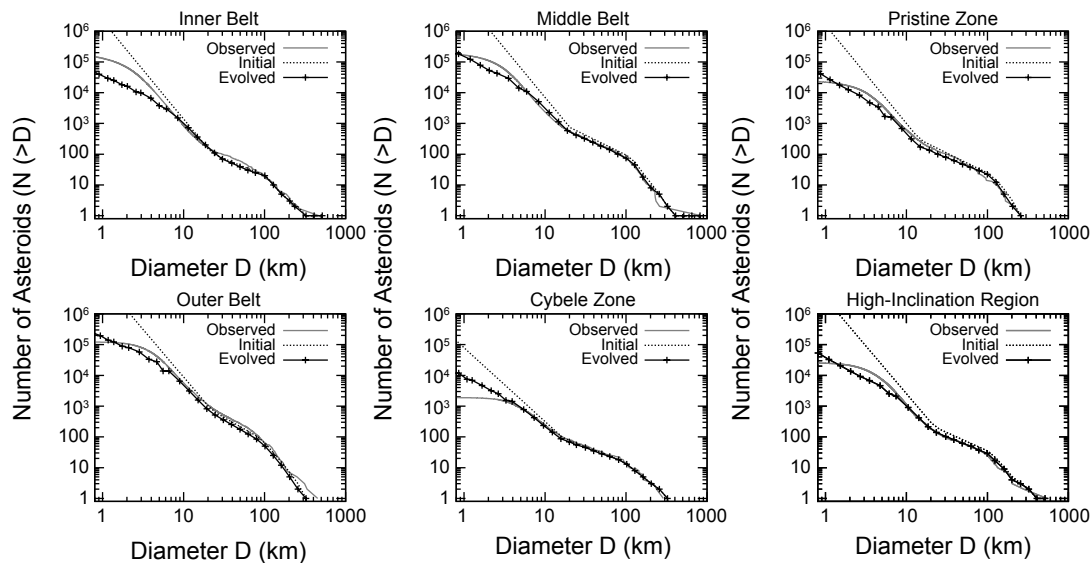


Fig. 9. Observed size-frequency distributions (gray lines) for six parts of the main belt compared to simulated initial (dashed) and final SFDs (black), after 4 G.y. of collisional evolution. This particular simulation shows the best-fit model out of more than 200,000 models started with various initial conditions. We assumed the scaling law of *Benz and Asphaug* (1999) and a monolithic structure of bodies. The largest differences can be seen for the inner and outer belt; they can be attributed to a dynamical removal of small bodies ($D < 0.1$ km) caused by the Yarkovsky effect, which then cannot serve as projectiles for larger bodies (≈ 1 km). Note that it is not easy to improve these results (e.g., by increasing the normalization of the outer belt; this would feed back and affect the other subpopulations). Figure adapted from *Cibulková et al.* (2014).

this number is reduced to as few as ~ 30 parent bodies. This large difference in numbers is even more puzzling given current meteorite delivery scenarios, where nearly any small main-belt fragment can potentially reach a resonance capable of taking it into the terrestrial planet region via the Yarkovsky effect (see the chapter by Vokrouhlický et al. in this volume). Presumably, this would suggest that our meteorite collections should have samples from thousands upon thousands of distinct parent bodies.

An important missing component here is information on how collisional evolution has shaped meteorite delivery in the asteroid belt. Using the models discussed above, it is useful to apply what we have learned to the issue of stony meteoroid production, evolution, and delivery to Earth. First, one can consider what happens when a body undergoes a cratering or catastrophic disruption event. A fragment SFD is created ranging from meteoroid-sized bodies all the way to multi-kilometer-sized asteroids (or more). Subsequent collisions onto bodies in the SFD act as a source for new meteoroids that are genetically the same as those created in the previous generation. This collisional cascade guarantees that some meteoroids from this family, representing a single parent body, will be provided to the main-belt population, resonances, and possibly to Earth for an extended interval. At the same time, dynamical processes and collisions onto the newly created meteoroids act as a sink to eliminate them from the main belt.

An example of this process is shown in Fig. 10. It shows what happens when fragment SFDs produced by $D = 30$ -km and 100 -km parent bodies are placed in the main belt

~ 3.1 G.y. ago. For fragments derived from the 30 -km body, the initial meteoroid population (i.e., the population of meter-sized bodies) drops by a factor of 100 and 10^5 within 130 m.y. and within 3.1 G.y., respectively. Thus, meteoroid production by $D < 30$ -km parent bodies decays away so quickly that breakup events of this size from billions of years ago are unlikely to deliver meaningful numbers of meteoroids to Earth today. For the 100 -km parent body, the decay rate is significantly slower, with the meteoroid population only dropping by a factor of 100 over 2 – 3 G.y. This suggests that many meteoroids reaching Earth today could come from prominent asteroid families with sizable SFDs, even if those families were created billions of years ago.

Bottke et al. (2005c) used these ideas to estimate how many stony meteorite classes should be in our collection. They did this by computing the meteoroid decay rates taken from different parent body sizes (Fig. 11) and combining them with the estimated production rates of asteroid families over the last ~ 4 G.y. This calculation made many simplifying assumptions: (1) meteoroids from all parts of the main belt have an equal chance of reaching Earth, (2) all $D > 30$ -km asteroids disrupted over the last several billion years have the capability of producing a distinct class of meteorites, and (3) once a family's meteoroid production rate drops by a factor of 100 , an arbitrary choice, it was unlikely to produce enough terrestrial meteorites to be noticed in our collection.

They found that asteroid families produced by the breakup of $D > 100$ -km bodies have such slow meteoroid decay rates that most should be providing some meteoroids today, regardless of their disruption time over the last 3 G.y. Among the

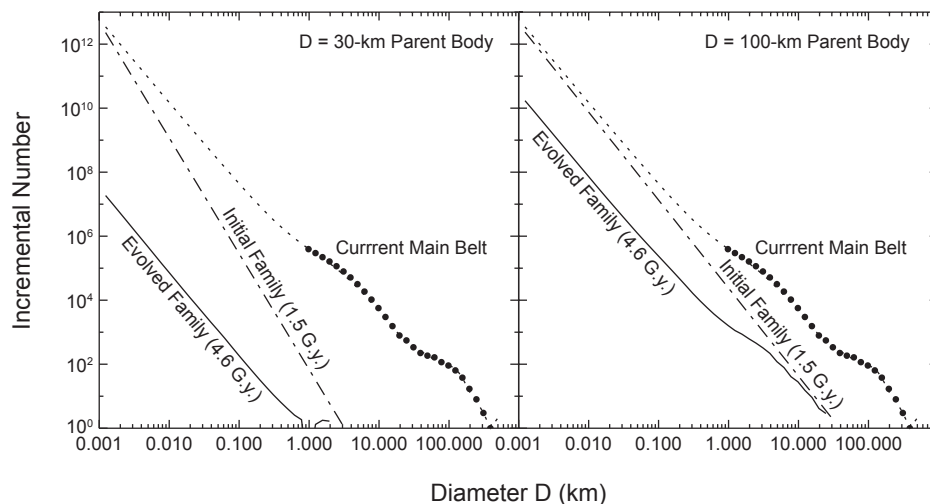


Fig. 10. The collisional and dynamical evolution of two asteroid families with simple fragment SFDs produced by the disruption of $D = 30$ - and 100 -km parent bodies (Bottke et al., 2005c). Both were inserted into the collision evolution model at 1.5 G.y. after solar system formation. The meteoroid population is represented by the number of bodies in the $D \sim 0.001$ -km size bin. The solid lines show the families at present (4.6 G.y.). The smaller family has decayed significantly more than the larger family. Note the shallow slope of the $D = 100$ -km family for $0.7 \leq D \leq 5$ km. This shape mimics that of the background main-belt population over the same size range.

smaller parent bodies ($30 < D < 100$ km), they found that, on average, the interval between disruption events across the main belt was short enough that many have disrupted over the last billion years or so, enough to provide some meteoroids as well. They did not examine large cratering events, such as the Rheasilvia formation event on Vesta, but presumably they would factor into this as well, with the biggest events acting like the disruption of a sizable parent body.

Overall, they found that stony meteorites were plausibly coming from ~ 45 different parent bodies. This value is fairly close to the actual value of ~ 30 parent bodies. A few reasons that the model estimate may be on the high side include (1) some disruption events must occur within existing families, so no unique meteorite class would be created; (2) some outer main-belt meteoroids may have great difficulty reaching Earth because they only have access to resonances that are orders of magnitude less efficient at delivering meteoroids to Earth than inner-main-belt resonances (Gladman *et al.*, 1997; Bottke *et al.*, 2006); and (3) we have not factored in the different fragment SFD actual families can have. We conclude that most stony meteorites are byproducts of a collisional cascade, with some coming from asteroid families produced by the breakup of $D > 100$ -km bodies over the last several billion years and the remainder coming from smaller, more recent breakup events among $D < 100$ -km asteroids that occurred over recent times (i.e., $\ll 1$ G.y.).

4.7. Cometary Impacts on Main-Belt Asteroids During the Late Heavy Bombardment

An interesting quandary comes from the predicted bombardment of comets on main-belt asteroids during the Nice model (see the chapter by Morbidelli *et al.* in this volume). Ac-

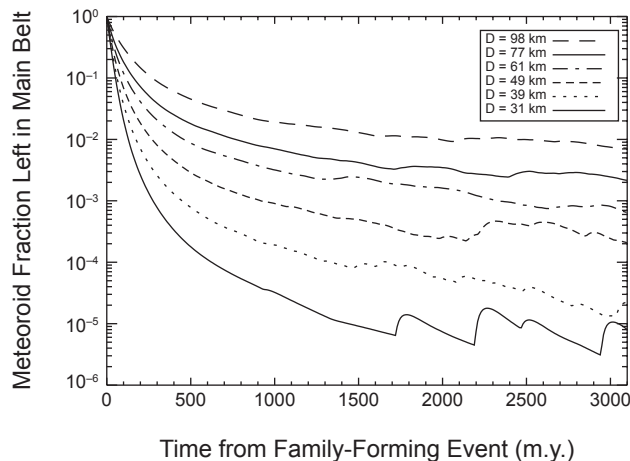


Fig. 11. Decay rates of meteoroid populations from asteroid families with simple power-law fragment SFD produced from parent bodies between $30 < D < 100$ km. All families were inserted in the collisional model at 3.1 G.y. ago. The meteoroid population in the smallest families decrease by a factor of 100 over a few 0.1 G.y. while the largest take several gigayears to decay by the same factor.

ording to Brož *et al.* (2013), a massive $25 M_{\oplus}$ disk of transneptunian comets might contain 10^{12} $D > 1$ -km comets. Using numerical simulations of Vokrouhlický *et al.* (2008), they estimated the collision probabilities and impact velocities for a comet hitting main-belt asteroids to be $P_1 \sim 6 \times 10^{-18} \text{ km}^{-2} \text{ yr}^{-1}$ and $V_{\text{imp}} \sim 10 \text{ km s}^{-1}$. Coupled with models describing the loss of asteroids during resonance sweeping (Minton and Malhotra, 2010), they estimated that the LHB could potentially disrupt more than 100 parent bodies with $D_{\text{PB}} > 100$ km, depending on the assumptions made (Fig. 12).

These values would violate many of the constraints provided in section 3, and they present an intriguing challenge to the main tenets of the Nice model. One option here would be to reject the Nice model altogether, although this would also mean giving up the successes it has had in explaining various solar system attributes (see the chapter by Morbidelli *et al.* in this volume).

The other possibility is that there are aspects of the Nice model or our collision models that need revision. For example, the disk of transneptunian comets may have different initial conditions and/or evolution properties than have been previously assumed, such that the collision probabilities between comets and asteroids are lower than expected (D. Nesvorný, personal communication). It is also possible that numerous transneptunian comets disrupt when they enter the inner solar system (e.g., Levison *et al.*, 2001), with possible mechanisms being volatile pressure buildup, amorphous/crystalline phase transitions, spinup by jets, etc. Brož *et al.* (2013) examined this possibility by arbitrarily assuming that all comets disrupt at perihelion distance, $q_{\text{crit}} < 1.5$ AU. On average, this led to the correct number of catastrophic disruptions for $D_{\text{PB}} = 200$ –400-km bodies, but it still pro-

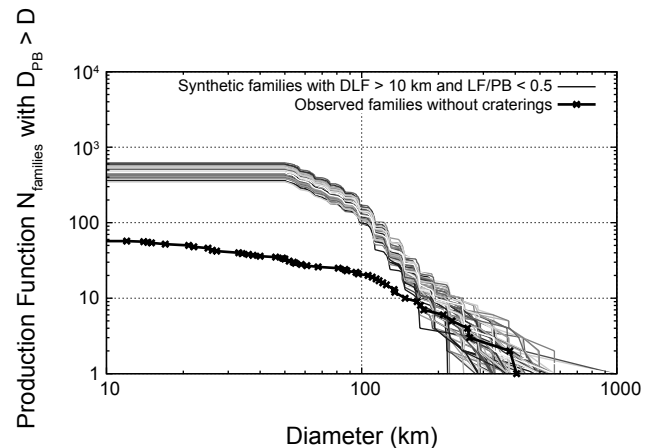


Fig. 12. The outcomes of the bombardment of the main asteroid belt by transneptunian comets, as modeled by Brož *et al.* (2013). The plot shows the family production functions [i.e., the cumulative number $N_{\text{fam}}(>D)$ of families with parent-body size D_{PB} larger than D] and a comparison to the observed one. Here we show 100 individual simulations (differing only by random-seed values) using different grayscale colors.

duced a factor of 2–3 more disruptions for $D_{PB} \approx 100$ -km bodies than observed. It is possible that this excess could be removed by subsequent collisional and dynamical evolution. All these values assume, of course, that collisions between low-density porous comets and asteroids are understood, when in reality no hydrocode simulations have ever been run using this set up. Finally, it could be that the main belt can accommodate more early collisions than predicted here. The constraints we have on the early era are extremely limited. All these topics remain exciting areas for future research.

5. CONCLUSIONS

Considerable progress has been made over the last several decades in interpreting how the main belt reached its current state by collisional and dynamical evolution, but there is still much work to do. At this time, no model has yet included all the important processes affecting asteroid evolution. Even after this accomplished, these models will still have to be successfully tested against all the known constraints, including new ones that are discussed in other chapters. Still, it is fair to say that many existing models have done a good job of matching the constraints discussed in section 3, and their predictions have made it possible to glean insights into how the main-belt population reached its current state (see section 4).

We expect that major advances will also come from the inclusion of new and better constraints that can help modelers rule out solutions. A few of the entries on our wish list for new data, beyond advances in the fields of planetesimal and planet formation, include (1) increased information on the main-belt population for $D < 1$ -km bodies (e.g., albedos, colors, spectroscopy, sizes, etc.); (2) a substantiated chronology for lunar and terrestrial crater populations, with crater SFD information verified for a wide range of surface ages; (3) a thorough examination of the main belt for ghost families; (4) more information on small asteroids that enable better predictions of Yarkovsky drift rates and YORP torques for $D < 1$ -km asteroids; (5) additional nonsaturated crater SFDs from asteroid surfaces; (6) more discoveries of very young families, enough that we convince ourselves we have a complete set for a given time period.

In regard to modeling work, the next major steps forward will probably come from next-generation codes that can track how asteroid populations move across the main belt via Yarkovsky/YORP forces while also undergoing comminution and YORP-driven mass shedding. This would allow the collisional cascade in the main belt to be treated as accurately as possible, from disruption all the way to the fragments reaching resonances. Additional information on asteroid collisions at all sizes from numerical hydrocode simulations would be extremely useful, as would laboratory and numerical experiments completed on a wide range of asteroid compositions and internal structures. This would allow new codes to accurately account for the varying Q_D^* functions and fragment SFDs that asteroid families of different composition might have.

Finally, it is imperative that collisional models employ the best estimates of how the main-belt and external small-body populations have dynamically evolved with time. The history of our solar system is etched into the main-belt population in enumerable ways, and the only way to read these markings and tell the story of our home is to unite models of collisional and dynamical evolution from the formation of the first solids all the way to the present day.

Acknowledgments. We thank reviewers E. Asphaug and F. Marzari for their helpful and constructive comments. Research funds for W.F.B. and S.M. were provided by NASA's Solar System Evolution Research Virtual Institute (SSERVI) as part of the Institute for the Science of Exploration Targets (ISET) at the Southwest Research Institute (NASA grant no. NNA14AB03A). The work of M.B. was supported by the Czech Grant Agency (grant no. P209-12-01308S).

REFERENCES

- Anders E. (1965) Fragmentation history of asteroids. *Icarus*, 4, 399–408.
- Asphaug E. (1997) Impact origin of the Vesta family. *Meteoritics & Planet. Sci.*, 32, 965–980.
- Asphaug E., Ryan E. V., and Zuber M. T. (2002) Asteroid interiors. In *Asteroids III* (W. F. Bottke Jr. et al., eds.), pp. 463–484. Univ. of Arizona, Tucson.
- Ballouz R.-L., Richardson D. C., Michel P., and Schwartz S. R. (2014) Rotation-dependent catastrophic disruption of gravitational aggregates. *Astrophys. J.*, 789, 158.
- Benavidez P. G., Durda D. D., Enke B. L., Bottke W. F., Nesvorný D., Richardson D. C., Asphaug E., and Merline W. J. (2012) A comparison between rubble-pile and monolithic targets in impact simulations: Application to asteroid satellites and family size distributions. *Icarus*, 219, 57–76.
- Benz W. and Asphaug E. (1999) Catastrophic disruptions revisited. *Icarus*, 142, 5–20.
- Bottke W. F. and Chapman C. R. (2006) Determining the main belt size distribution using asteroid crater records and crater saturation models. *Lunar Planet. Sci. XXXVII*, Abstract #1349. Lunar and Planetary Institute, Houston.
- Bottke W. F., Nolan M. C., Greenberg R., and Kolvoord R. A. (1994) Velocity distributions among colliding asteroids. *Icarus*, 107, 255–268.
- Bottke W. F., Durda D. D., Nesvorný D., Jedicke R., Morbidelli A., Vokrouhlický D., and Levison H. (2005a) The fossilized size distribution of the main asteroid belt. *Icarus*, 175, 111–140.
- Bottke W. F., Durda D. D., Nesvorný D., Jedicke R., Morbidelli A., Vokrouhlický D., and Levison H. F. (2005b) Linking the collisional history of the main asteroid belt to its dynamical excitation and depletion. *Icarus*, 179, 63–94.
- Bottke W. F., Durda D. D., Nesvorný D., Jedicke R., Morbidelli A., Vokrouhlický D., and Levison H. F. (2005c) The origin and evolution of stony meteorites. In *Dynamics of Populations of Planetary Systems* (Z. Knežević and A. Milani, eds.), pp. 357–374. Cambridge Univ., Cambridge.
- Bottke W. F., Nesvorný D., Grimm R. E., Morbidelli A., and O'Brien D. P. (2006) Iron meteorites as remnants of planetesimals formed in the terrestrial planet region. *Nature*, 439, 821–824.
- Bottke W. F., Levison H. F., Nesvorný D., and Dones L. (2007) Can planetesimals left over from terrestrial planet formation produce the lunar late heavy bombardment? *Icarus*, 190, 203–223.
- Bottke W. F., Vokrouhlický D., Minton D., Nesvorný D., Morbidelli A., Brasser R., Simonson B., and Levison H. F. (2012) An Archaean heavy bombardment from a destabilized extension of the asteroid belt. *Nature*, 485, 78–81.
- Bottke W. F. et al. (2015a) In search of the source of asteroid (101955) Bennu: Applications of the stochastic YORP model. *Icarus*, 247, 191–271.
- Bottke W. F., Vokrouhlický D., Marchi S., Swindle T., Scott E. R. D., Weirich J., and Levison H. (2015b) Dating the Moon-forming impact event with asteroidal meteorites. *Science*, 348, 321–323.

- Brasser R., Morbidelli A., Gomes R., Tsiganis K., and Levison H. F. (2009) Constructing the secular architecture of the solar system II: The terrestrial planets. *Astron. Astrophys.*, 507, 1053–1065.
- Britt D. T., Yeomans D., Housen K., and Consolmagno G. (2002) Asteroid density, porosity, and structure. In *Asteroids III* (W. F. Bottke Jr. et al., eds.), pp. 485–500. Univ. of Arizona, Tucson.
- Brown P. G., et al. (2013) A 500-kiloton airburst over Chelyabinsk and an enhanced hazard from small impactors. *Nature*, 503, 238–241.
- Brož M., Morbidelli A., Bottke W. F., Rozehnal J., Vokrouhlický D., and Nesvorný D. (2013) Constraining the cometary flux through the asteroid belt during the late heavy bombardment. *Astron. Astrophys.*, 551, A117.
- Buczkowski D. L. et al. (2012) Large-scale troughs on Vesta: A signature of planetary tectonics. *Geophys. Res. Lett.*, 39, L18205.
- Burbine T. H., McCoy T. J., Meibom A., Gladman B., and Keil K. (2002) Meteoritic parent bodies: Their number and identification. In *Asteroids III* (W. F. Bottke Jr. et al., eds.), pp. 653–667. Univ. of Arizona, Tucson.
- Carruba V., Burns J. A., Bottke W., and Nesvorný D. (2003) Orbital evolution of the Gefion and Adeona asteroid families: Close encounters with massive asteroids and the Yarkovsky effect. *Icarus*, 162, 308–327.
- Carruba V., Huaman M., Domingos R. C., and Roig F. (2013) Chaotic diffusion caused by close encounters with several massive asteroids. II. The regions of (10) Hygiea, (2) Pallas, and (31) Euphrosyne. *Astron. Astrophys.*, 550, A85.
- Campo Bagatin A., Cellino A., Davis D. R., Farinella P., and Paolicchi P. (1994) Wavy size distributions for collisional systems with a small-size cutoff. *Planet. Space Sci.*, 42, 1079–1092.
- Campo Bagatin A., Petit J.-M., and Farinella P. (2001) How many rubble piles are in the asteroid belt? *Icarus*, 149, 198–209.
- Cibulková H., Brož M., and Benavidez P. G. (2014) A six-part collisional model of the main asteroid belt. *Icarus*, 241, 358–372.
- Cotto-Figueroa D. (2013) Radiation recoil effects on the dynamical evolution of asteroids. Ph.D. thesis, Ohio University, Athens, Ohio.
- Cotto-Figueroa D., Statler T. S., Richardson D. C., and Tanga P. (2015) Coupled spin and shape evolution of small rubble-pile asteroids: Self-limitation of the YORP effect. *Astrophys. J.*, 803, 25.
- Chambers J. E. and Wetherill G. W. (1998) Making the terrestrial planets: N-body integrations of planetary embryos in three dimensions. *Icarus*, 136, 304–327.
- Chambers J. E. and Wetherill G. W. (2001) Planets in the asteroid belt. *Meteoritics & Planet. Sci.*, 36, 381–399.
- Dale C. W., Burton K. W., Greenwood R. C., Gannoun A., Wade J., Wood B. J., and Pearson D. G. (2012) Late accretion on the earliest planetesimals revealed by the highly siderophile elements. *Science*, 336, 72–75.
- Davison T. M., O'Brien D. P., Ciesla F. J., and Collins G. S. (2013) The early impact histories of meteorite parent bodies. *Meteoritics & Planet. Sci.*, 48, 1894–1918.
- Davis D. R., Chapman C. R., Greenberg R., Weidenschilling S. J., and Harris A. W. (1979) Collisional evolution of asteroids — populations, rotations, and velocities. In *Asteroids* (T. Gehrels, ed.), pp. 528–557. Univ. of Arizona, Tucson.
- Davis D. R., Chapman C. R., Weidenschilling S. J., and Greenberg R. (1985) Collisional history of asteroids: Evidence from Vesta and the Hirayama families. *Icarus*, 63, 30–53.
- Davis D. R., Weidenschilling S. J., Farinella P., Paolicchi P., and Binzel R. P. (1989) Asteroid collisional history — effects on sizes and spins. In *Asteroids II* (R. P. Binzel et al., eds.), pp. 805–826. Univ. of Arizona, Tucson.
- Davis D. R., Durda D. D., Marzari F., Campo Bagatin A., and Gil-Hutton R. (2002) Collisional evolution of small body populations. In *Asteroids III* (W. F. Bottke Jr. et al., eds.), pp. 545–558. Univ. of Arizona, Tucson.
- Dell'Oro A. and Paolicchi P. (1998) Statistical properties of encounters among asteroids: A new, general purpose, formalism. *Icarus*, 136, 328–339.
- Dohnanyi J. W. (1969) Collisional models of asteroids and their debris. *J. Geophys. Res.*, 74, 2531–2554.
- Durda D. D. and Dermott S. F. (1997) The collisional evolution of the asteroid belt and its contribution to the zodiacal cloud. *Icarus*, 130, 140–164.
- Durda D. D., Greenberg R., and Jedicke R. (1998) Collisional models and scaling laws: A new interpretation of the shape of the main-belt asteroid size distribution. *Icarus*, 135, 431–440.
- Durda D. D., Bottke W. F., Enke B. L., Merline W. J., Asphaug E., Richardson D. C., and Leinhardt Z. M. (2004) The formation of asteroid satellites in large impacts: Results from numerical simulations. *Icarus*, 170, 243–257.
- Durda D. D. et al. (2007) Size-frequency distributions of fragments from SPH/N-body simulations of asteroid impacts: Comparison with observed asteroid families. *Icarus*, 186, 498–516.
- Eugster O. (2003) Cosmic-ray exposure ages of meteorites and lunar rocks and their significance. *Chem. Erde*, 63, 3–30.
- Farinella P. and Davis D. R. (1992) Collision rates and impact velocities in the main asteroid belt. *Icarus*, 97, 111–123.
- Farinella P., Davis D. R., Paolicchi P., Cellino A., and Zappala V. (1992) Asteroid collisional evolution — an integrated model for the evolution of asteroid rotation rates. *Astron. Astrophys.*, 253, 604–614.
- Fowler J. W. and Chillemi J. R. (1992) IRAS asteroid data processing. In *The IRAS Minor Planet Survey* (E. F. Tedesco, ed.), pp. 17–43. Tech. Report PL-TR-92-2049, Phillips Laboratory, Hanscom Air Force Base, Massachusetts.
- Golubov O. and Krugly Y. N. (2012) Tangential component of the YORP effect. *Astrophys. J. Lett.*, 752, L11.
- Golubov O., Scheeres D. J., and Krugly Y. N. (2014) A three dimensional model of tangential YORP. *Astrophys. J.*, 794, 22.
- Gomes R., Levison H. F., Tsiganis K., and Morbidelli A. (2005) Origin of the cataclysmic late heavy bombardment period of the terrestrial planets. *Nature*, 435, 466–469.
- Gladman B. J., Migliorini F., Morbidelli A., Zappala V., Michel P., Cellino A., Froeschle C., Levison H. F., Bailey M., and Duncan M. (1997) Dynamical lifetimes of objects injected into asteroid belt resonances. *Science*, 277, 197–201.
- Gladman B. J. et al. (2009) On the asteroid belt's orbital and size distribution. *Icarus*, 202, 104–118.
- Hanuš J. et al. (2013) Asteroids' physical models from combined dense and sparse photometry and scaling of the YORP effect by the observed obliquity distribution. *Astron. Astrophys.*, 551, A67.
- Hartmann W. K. and Hartmann A. C. (1968) Asteroid collisions and evolution of asteroidal mass distribution and meteoritic flux. *Icarus*, 8, 361–381.
- Hiesinger H., van der Bogert C. H., Pasckert J. H., Funcke L., Giacomini L., Ostrach L. R., and Robinson M. S. (2012) How old are young lunar craters? *J. Geophys. Res.—Planets*, 117, E00H10.
- Holsapple K., Giblin I., Housen K., Nakamura A., and Ryan E. (2002) Asteroid impacts: Laboratory experiments and scaling laws. In *Asteroids III* (W. F. Bottke Jr. et al., eds.), pp. 443–462. Univ. of Arizona, Tucson.
- Housen K. (2009) Cumulative damage in strength-dominated collisions of rocky asteroids: Rubble piles and brick piles. *Planet. Space Sci.*, 57, 142–153.
- Ivezić Ž. et al. (2001) Solar system objects observed in the Sloan digital sky survey commissioning data. *Astron. J.*, 122, 2749–2784.
- Ivanov B. A., Neukum G., Bottke W. F., and Hartmann W. K. (2002) The comparison of size-frequency distributions of impact craters and asteroids and the planetary cratering rate. In *Asteroids III* (W. F. Bottke Jr. et al., eds.), pp. 90–101. Univ. of Arizona, Tucson.
- Jacobson S. A., Marzari F., Rossi A., Scheeres D. J., and Davis D. R. (2014) Effect of rotational disruption on the size frequency distribution of the main belt asteroid population. *Mon. Not. R. Astron. Soc.*, 439, L95–L99.
- Jaumann R. et al. (2012) Vesta's shape and morphology. *Science*, 336, 687–690.
- Jedicke R., Larsen J., and Spahr T. (2002) Observational selection effects in asteroid surveys. In *Asteroids III* (W. F. Bottke Jr. et al., eds.), pp. 71–88. Univ. of Arizona, Tucson.
- Jutzi M., Asphaug E., Gillet P., Barrat J.-A., and Benz W. (2013) The structure of the asteroid 4 Vesta as revealed by models of planet-scale collisions. *Nature*, 494, 207–210.
- Kirchoff M. R., Chapman C. R., Marchi S., Curtis K. M., Enke B., and Bottke W. F. (2013) Ages of large lunar impact craters and implications for bombardment during the Moon's middle age. *Icarus*, 225, 325–341.

- Krasinsky G. A., Pitjeva E. V., Vasilyev M. V., and Yagudina E. I. (2002) Hidden mass in the asteroid belt. *Icarus*, 158, 98–105.
- Kuchynka P. and Folkner W. M. (2013) A new approach to determining asteroid masses from planetary range measurements. *Icarus*, 222, 243–253.
- Kuiper G. P., Fugita Y. F., Gehrels T., Groeneveld I., Kent J., van Biesbroeck G., and van Houten C. J. (1958) Survey of asteroids. *Astrophys. J. Suppl.*, 3, 289.
- Leinhardt Z. M. and Stewart S. T. (2009) Full numerical simulations of catastrophic small body collisions. *Icarus*, 199, 542–559.
- Leinhardt Z. M. and Stewart S. T. (2012) Collisions between gravity dominated bodies. I. Outcome regimes and scaling laws. *Astrophys. J.*, 745, 79.
- Levison H. F., Dones L., Chapman C. R., Stern S. A., Duncan M. J., and Zahnle K. (2001) Could the lunar “late heavy bombardment” have been triggered by the formation of Uranus and Neptune? *Icarus*, 151, 286–306.
- Levison H. F., Bottke W. F., Gounelle M., Morbidelli A., Nesvorný D., and Tsiganis K. (2009) Contamination of the asteroid belt by primordial trans-Neptunian objects. *Nature*, 460, 364–366.
- Levison H. F., Kretke K. A., Walsh K., and Bottke W. F. (2015a) Growing the terrestrial planets from the slow accumulation of sub-meter-size objects. *Proc. Natl. Acad. Sci.*, in press.
- Levison H. F., Kretke K. A., and Duncan M. J. (2015b) Growing the gas giant planets from the slow accumulation of centimeter- to meter-size objects. *Nature*, 524, 322–324.
- Love S. G. and Ahrens T. J. (1997) Origin of asteroid rotation rates in catastrophic impacts. *Nature*, 386, 154–156.
- Manley S. P., Migliorini F., and Bailey M. E. (1998) An algorithm for determining collision probabilities between small solar system bodies. *Astronomy Astrophys. Suppl.*, 133, 437–444.
- Marchi S., Mottola S., Cremonese G., Massironi M., and Martellato E. (2009) A new chronology for the Moon and Mercury. *Astron. J.*, 137, 4936–4948.
- Marchi S. et al. (2012) The violent collisional history of asteroid 4 Vesta. *Science*, 336, 690–693.
- Marchi S. et al. (2013) High-velocity collisions from the lunar cataclysm recorded in asteroidal meteorites. *Nature Geosci.*, 6, 303–307.
- Marchi S. et al. (2014) Small crater populations on Vesta. *Planet. Space Sci.*, 103, 96–103.
- Marzari F., Rossi A., and Scheeres D. J. (2011) Combined effect of YORP and collisions on the rotation rate of small main belt asteroids. *Icarus*, 214, 622–631.
- Masiero J. et al. (2011) Main belt asteroids with WISE/NEOWISE I: Preliminary albedos and diameters. *Astrophys. J.*, 741, 68.
- McEwen A. S., Moore J. M., and Shoemaker E. M. (1997) The Phanerozoic impact cratering rate: Evidence from the far side of the Moon. *J. Geophys. Res.*, 102, 9231–9242.
- Melosh H. J. (1989) *Impact Cratering: A Geologic Process*. Oxford Univ., New York. 253 pp.
- Merline W. J., Weidenschilling S. J., Durda D. D., Margot J. L., Pravec P., and Storrs A. D. (2002) Asteroids do have satellites. In *Asteroids III* (W. F. Bottke Jr. et al., eds.), pp. 289–312. Univ. of Arizona, Tucson.
- Minton D. A. and Malhotra R. (2009) A record of planet migration in the main asteroid belt. *Nature*, 457, 1109–1111.
- Minton D. A. and Malhotra R. (2010) Dynamical erosion of the asteroid belt and implications for large impacts in the inner solar system. *Icarus*, 207, 744–757.
- Minton D. A. and Malhotra R. (2011) Secular resonance sweeping of the main asteroid belt during planet migration. *Astrophys. J.*, 732, 53.
- Morbidelli A. and Gladman B. (1998) Orbital and temporal distributions of meteorites originating in the asteroid belt. *Meteoritics & Planet. Sci.*, 33, 999–1016.
- Morbidelli A. and Vokrouhlický D. (2003) The Yarkovsky-driven origin of near-Earth asteroids. *Icarus*, 163, 120–134.
- Morbidelli A., Bottke W. F., Nesvorný D., and Levison H. F. (2009) Asteroids were born big. *Icarus*, 204, 558–573.
- Morbidelli A., Brasser R., Gomes R., Levison H. F., and Tsiganis K. (2010) Evidence from the asteroid belt for a violent past evolution of Jupiter’s orbit. *Astron. J.*, 140, 1391–1401.
- Morbidelli A., Marchi S., Bottke W. F., and Kring D. A. (2012) A sawtooth-like timeline for the first billion years of lunar bombardment. *Earth Planet. Sci. Lett.*, 355, 144–151.
- Nesvorný D. (2011) Young solar system’s fifth giant planet? *Astrophys. J. Lett.*, 742, L22.
- Nesvorný D. and Bottke W. F. (2004) Detection of the Yarkovsky effect for main-belt asteroids. *Icarus*, 170, 324–342.
- Nesvorný D. and Morbidelli A. (2012) Statistical study of the early solar system’s instability with four, five, and six giant planets. *Astron. J.*, 144, 117.
- Nesvorný D., Morbidelli A., Vokrouhlický D., Bottke W. F., and Brož M. (2002) The Flora family: A case of the dynamically dispersed collisional swarm? *Icarus*, 157, 155–172.
- Nesvorný D., Bottke W. F., Levison H., and Dones L. (2003) Recent origin of the solar system dust bands. *Astrophys. J.*, 591, 486–497.
- Nesvorný D., Roig F., Gladman B., Lazzaro D., Carruba V., and Mothé-Diniz T. (2008) Fugitives from the Vesta family. *Icarus*, 193, 85–95.
- Novaković B., Dell’Oro A., Cellino A., and Knežević Z. (2012) Recent collisional jet from a primitive asteroid. *Mon. Not. R. Astron. Soc.*, 425, 338–346.
- Novaković B., Hsieh H. H., Cellino A., Micheli M., and Pedani M. (2014) Discovery of a young asteroid cluster associated with P/2012 F5 (Gibbs). *Icarus*, 231, 300–309.
- O’Brien D. P. (2009) The Yarkovsky effect is not responsible for small crater depletion on Eros and Itokawa. *Icarus*, 203, 112–118.
- O’Brien D. P. and Greenberg R. (2003) Steady-state size distributions for collisional populations: Analytical solution with size dependent strength. *Icarus*, 164, 334–345.
- O’Brien D. P. and Greenberg R. (2005) The collisional and dynamical evolution of the main-belt and NEA size distributions. *Icarus*, 178, 179–212.
- O’Brien D. P., Morbidelli A., and Levison H. F. (2006) Terrestrial planet formation with strong dynamical friction. *Icarus*, 184, 39–58.
- O’Brien D. P., Morbidelli A., and Bottke W. F. (2007) The primordial excitation and clearing of the asteroid belt — revisited. *Icarus*, 191, 43–452.
- Öpik E. J. (1951) Collision probability with the planets and the distribution of planetary matter. *Proc. R. Irish Acad.*, 54, 165–199.
- Parker A., Ivezić Ž., Jurić M., Lupton R., Sekora M. D., and Kowalski A. (2008) The size distributions of asteroid families in the SDSS Moving Object Catalog 4. *Icarus*, 198, 138–155.
- Penco U., Dell’Oro A., Paolicchi P., Campo Bagatin A., La Spina A., and Cellino A. (2004) Yarkovsky depletion and asteroid collisional evolution. *Planet. Space Sci.*, 52, 1087–1091.
- Petit J. M. and Farinella P. (1993) Modelling the outcomes of high-velocity impacts between small solar system bodies. *Cel. Mech. Dyn. Astron.*, 57, 1–28.
- Petit J., Chambers J., Franklin F., and Nagasawa M. (2002) Primordial excitation and depletion of the main belt. In *Asteroids III* (W. F. Bottke Jr. et al., eds.), pp. 711–738. Univ. of Arizona, Tucson.
- Pravec P., Harris A. W., and Michalowski T. (2002) Asteroid rotations. In *Asteroids III* (W. F. Bottke Jr. et al., eds.), pp. 113–122. Univ. of Arizona, Tucson.
- Rabinowitz D. L., Helin E., Lawrence K., and Pravdo S. (2000) A reduced estimate of the number of kilometre-sized near-Earth asteroids. *Nature*, 403, 165–166.
- Robbins S. J. (2014) New crater calibrations for the lunar craterage chronology. *Earth Planet. Sci. Lett.*, 403, 188–198.
- Rozitis B. and Green S. F. (2012) The influence of rough surface thermal-infrared beaming on the Yarkovsky and YORP effects. *Mon. Not. R. Astron. Soc.*, 423, 367–388.
- Ryder G., Bogard D., and Garrison D. (1991) Probable age of Autolycus and calibration of lunar stratigraphy. *Geology*, 19, 143–146.
- Schenk P. et al. (2012) The geologically recent giant impact basins at Vesta’s south pole. *Science*, 336, 694–697.
- Slivan S. M. (2002) Spin vector alignment of Koronis family asteroids. *Nature*, 419, 49–51.
- Slivan S. M. and Molnar L. A. (2012) Spin vectors in the Koronis family: III. (832) Karin. *Icarus*, 220, 1097–1103.
- Slivan S. M., Binzel R. P., Crespo da Silva L. D., Kaasalainen M., Lyndaker M. M., and Krčo M. (2003) Spin vectors in the Koronis family: Comprehensive results from two independent analyses of 213 rotation light curves. *Icarus*, 162, 285–307.

- Slivan S. M., Binzel R. P., Kaasalainen M., Hock A. N., Klesman A. J., Eckelman L. J., and Stephens R. D. (2009) Spin vectors in the Koronis family. II. Additional clustered spins, and one stray. *Icarus*, 200, 514–530.
- Statler T. S. (2009) Extreme sensitivity of the YORP effect to small-scale topography. *Icarus*, 202, 502–513.
- Stöffler D. and Ryder G. (2001) Stratigraphy and isotope ages of lunar geologic units: Chronological standard for the inner solar system. *Space Sci. Rev.*, 96, 9–54.
- Stokes G. H., Yeomans D. K., Bottke W. F., Chesley S. R., Evans J. B., Gold R. E., Harris A. W., Jewitt D., Kelso T. S., McMillan R. S., Spahr T. B., and Worden S. P. (2003) *Report of the Near-Earth Object Science Definition Team: A Study to Determine the Feasibility of Extending the Search for Near-Earth Objects to Smaller Limiting Diameters*. NASA OSS-Solar System Exploration Division, Washington, DC.
- Somenzi L., Fienga A., Laskar J., and Kuchynka P. (2010) Determination of asteroid masses from their close encounters with Mars. *Planet. Space Sci.*, 58, 858–863.
- Tanaka H., Inaba S., and Nakazawa K. (1996) Steady-state size distribution for the self-similar collision cascade. *Icarus*, 123, 450–455.
- Turrini D., Magni G., and Coradini A. (2011) Probing the history of solar system through the cratering records on Vesta and Ceres. *Mon. Not. R. Astron. Soc.*, 413, 2439–2466.
- Turrini D., Coradini A., and Magni G. (2012) Jovian early bombardment: Planetesimal erosion in the inner asteroid belt. *Astrophys. J.*, 750, 8.
- Vedder J. D. (1998) Main belt asteroid collision probabilities and impact velocities. *Icarus*, 131, 283–290.
- Vokrouhlický D., Nesvorný D., and Bottke W. F. (2003) The vector alignments of asteroid spins by thermal torques. *Nature*, 425, 147–151.
- Vokrouhlický D., Nesvorný D., and Levison H. F. (2008) Irregular satellite capture by exchange reactions. *Astron. J.*, 136, 1463–1476.
- Walsh K. J., Morbidelli A., Raymond S. N., O'Brien D. P., and Mandell A. M. (2011). A low mass for Mars from Jupiter's early gas-driven migration. *Nature*, 475, 206–209.
- Weidenschilling S. J. (1977) The distribution of mass in the planetary system and solar nebula. *Astrophys. Space Sci.*, 51, 153–158.
- Wetherill G. W. (1967) Collisions in the asteroid belt. *J. Geophys. Res.*, 72, 2429–2444.
- Wilhelms D. E. (1987) *The Geologic History of the Moon*. U.S. Geol. Surv. Prof. Paper 1348, 302 pp. Available online at <http://ser.sese.asu.edu/GHM/>.
- Wilhelms D. E., Oberbeck V. R., and Aggarwal H. R. (1978) Size-frequency distributions of primary and secondary lunar impact craters. *Lunar Planet. Sci. IX*, pp. 1256–1258. Lunar and Planetary Institute, Houston.
- Williams D. R. and Wetherill G. W. (1994) Size distribution of collisionally evolved asteroidal populations — analytical solution for self-similar collision cascades. *Icarus*, 107, 117–125.